uOttawa

# Adsorbent Screening for the Separation of $CO_2$, $CH_4$, and $N_2$

By
**Dana Li**

Thesis submitted to the University of Ottawa
in partial fulfillment of the requirements for the degree of
**Master of Applied Science in Chemical Engineering**

Supervisor
Dr. F. Handan Tezel

Department of Chemical and Biological Engineering
Faculty of Engineering
University of Ottawa

# Abstract

The objective of this research was to determine an appropriate adsorbent for the separation of $CH_4$ from $CO_2$, $N_2$, and $O_2$. To screen different adsorbents for this purpose, pure component adsorption isotherms and gas mixture isotherms were measured.

Adsorption isotherms are critical data for modeling adsorption processes. Thus, determining an accurate and reliable method of measuring gas adsorption isotherms is crucial. Concentration pulse chromatography can be used to measure the slope of the isotherm. In the case of pure component adsorption, the slope at different partial pressures of adsorbate can be integrated to determine the adsorption isotherm. The accuracy of the concentration pulse chromatography method was compared to that of gravimetric analysis to find an appropriate technique to obtain pure component gas adsorption isotherms by measuring $CH_4$ isotherms on activated carbon at 25°C and up to 6.3 atm. Isotherm results from concentration pulse chromatography were identical to gravimetric results, but the use of a sufficiently long column for concentration pulse chromatography was crucial.

Afterwards, gravimetric analysis was used to determine the performance of activated carbon (AC A-C) and carbon molecular sieve (CMS A-D) adsorbents for adsorbing $CO_2$ and $N_2$. Additionally, $O_2$ adsorption isotherms were measured for CMS's. At 25°C and above atmospheric pressure, AC-B showed the highest $CO_2$ capacity and $CO_2/N_2$ selectivity. The isosteric heat of adsorption values of $CO_2$, $N_2$, and $O_2$ for the CMS's were calculated; CMS-A and CMS-C had high isosteric heat of adsorption values for $CO_2$, above 40 kJ $mol^{-1}$.

Finally, the performance of activated carbon in separating a binary mixture of $CO_2$ and $N_2$ was experimentally measured by obtaining binary gas mixture adsorption isotherms using concentration pulse chromatography technique between 30-70°C and 1-5 atm total pressure. The OLC activated carbon showed selectivity for $CO_2$ over $N_2$, with the experimental results showing a slight deviation from theoretical predictions of the binary adsorption isotherms. Compared to other adsorbents in the literature, OLC had similar $CO_2$ and $N_2$ adsorption capacities but higher $CO_2/N_2$ selectivity.

# Sommaire

L'objectif de cette recherche était de déterminer un adsorbant pour la séparation du $CH_4$ du $CO_2$, $N_2$, et $O_2$. Pour filtrer des adsorbants pour ce but, des isothermes d'adsorption pour des composants purs, ainsi que pour des mélanges de gaz, étaient mesurés.

Les isothermes d'adsorption sont très importantes pour la modélisation des processus d'adsorption. Donc, une méthode précise et fiable pour la mesure des isothermes d'adsorptions de gaz est critique. La technique chromatographique d'une impulsion en concentration peut être utilisée pour mesurer la pente de l'isotherme. Dans le cas de l'adsorption d'un gaz pur, la pente à pressions partielles différents peut être intégrée pour déterminer l'isotherme d'adsorption. La précision de cette méthode a été comparée à l'analyse gravimétrique pour trouver une technique appropriée pour la mesure des isothermes $CH_4$ sur le charbon actif à 25°C et jusqu'à 6.3 atm. L'isotherme mesurée par la technique chromatographique d'une impulsion en concentration était identique à l'isotherme mesurée à l'analyse gravimétrique, mais l'utilisation d'une colonne suffisamment longue pour la technique chromatographique d'une impulsion en concentration a été cruciale.

Ensuite, l'analyse gravimétrique a été utilisée pour déterminer la capacité de $CO_2$ et $N_2$ pour des charbons actifs (AC A-C) et des tamis moléculaire de carbone (CMS A-D). Des isothermes d'$O_2$ ont aussi été mesurées pour les CMS. À 25°C et aux pressions au-dessus de la pression atmosphérique, AC-B a démontré la capacité de $CO_2$ la plus élevée ainsi que la sélectivité la plus élevée. Les valeurs de la chaleur isostérique d'adsorption de $CO_2$, $N_2$, et $O_2$ pour les CMS ont été calculées ; CMS-A et CMS-C avait des valeurs de la chaleur isostérique d'adsorption les plus élevées, de plus que 40 kJ $mol^{-1}$.

Finalement, la capacité pour la séparation d'un mélange binaire de $CO_2$ et $N_2$ d'un charbon actif a été mesurée par la technique chromatographique d'une impulsion en concentration entre 30-70°C et 1-5 atm pression totale. Le charbon actif OLC a démontré une sélectivité pour $CO_2$ sur $N_2$, avec une déviation légère des prédictions théoriques pour les isothermes d'adsorption binaire. Par rapport aux autres adsorbants dans la littérature, OLC avait des capacités de $CO_2$ et $N_2$ semblable, mais avait des meilleures sélectivités $CO_2/N_2$.

# Table of Contents

# I. List of Tables

## II. List of Figures

## III. Thesis Structure

This thesis consists of five chapters.

**Chapter 1** is a general introduction to concepts related to this work, which include adsorption, the gases tested, types of adsorbents, and the industrial application of the research.

**Chapter 2** pertains to the article named "Determination of adsorption isotherms using concentration pulse chromatography" which will be submitted to a scientific journal. The conditions required to measure accurate adsorption isotherms with concentration pulse chromatography are examined.

**Chapter 3** is a study on different adsorbents for the separation of $CO_2$ and $N_2$, titled "Adsorbent screening for $CO_2$ capture by pure component isotherm measurements". This chapter assesses the pure component adsorption capacities of activated carbon and carbon molecular sieves and predicts the $CO_2$-$N_2$ binary adsorption isotherms.

**Chapter 4** explores the effect of temperature and pressure on $CO_2$-$N_2$ binary adsorption isotherms on activated carbon, titled "Binary adsorption equilibria of $CO_2$-$N_2$ mixtures on activated carbon".

Finally, **Chapter 5** serves as an overall conclusion to the thesis, and provides several recommendations for future work.

## IV. Contribution of Collaborators

I hereby declare that I am the first author of this thesis. However, several collaborators helped contribute to the work presented.

In Chapter 2, Connor Francis assisted with collecting chromatographic adsorption data and analyzing the chromatograph peaks, and Dr. F. Handan Tezel collected the gravimetric adsorption data. Other data analysis was carried out by myself. I completed the single gas adsorption experiments and analysis in Chapter 3. In Chapter 4, the pure component gas adsorption isotherms were collected by Sean Wilson. The binary gas adsorption isotherm experiments and peak analysis were conducted by Connor Francis (40%) and myself (60%). I completed all other experiments and data analysis.

Dr. F. Handan Tezel helped make comments and corrections on the thesis manuscript, along with financial and technical support, as well as weekly meetings.

## V. Acknowledgments

First, I would like to thank my supervisor Dr. F. Handan Tezel, who helped guide and support me during my thesis. She was an invaluable mentor who imparted some of her chemical engineering knowledge to me, as well as other skills for my future career.

I would also like to thank the technical support staff at the Department of Chemical and Biological Engineering, Franco Ziraldo, Gérard Nina, James Macdermid, and Patrick Pageau for their help with modifying, troubleshooting, and repairing the laboratory equipment. The experimental work was made possible by them. Also, thanks to Antonio Toledo from TA Instruments, New Castle, DE, USA who helped repair the VTI Corp. gravimetric system.

I would like to recognize NSERC, Eco Canada, Mitacs, and the University of Ottawa for financial support during my studies through scholarships and internships. I would also like to thank our industrial partner Xebec Adsorption Inc. for financial support through the Mitacs Accelerate program.

Finally, I would like to thank my friends and family for their love and support. A special thanks to my siblings who always make me smile.

# Chapter 1 - Introduction

Anthropogenic activities have resulted in the emission of greenhouse gases, affecting global climate. $CO_2$ comprises the majority of these emissions, at about 75% of 59 Gt $CO_2$ equivalents in 2019, with a 1.3% increase in total greenhouse gas (GHG) emissions from anthropogenic sources from 2010 to 2019.[1] To mitigate the effects of climate change, many efforts have been exerted to using renewable energy sources and capturing carbon emissions.

Adsorption can be used for the separation of $CH_4$, $CO_2$, and $N_2$. Compared to other gas separation technologies like absorption or cryogenic distillation, adsorption can be less energy intensive, thus providing an economical benefit. When designing an adsorption process, there are several parameters that must be considered. In terms of selecting an adsorbent appropriate for separation of a given mixture, adsorption capacity, selectivity, kinetics, heat effects, and adsorbent regeneration are all important factors to consider. In this work, there is a focus on investigating the equilibrium adsorption capacity and selectivity of different adsorbents.

## 1.1 Natural Gas

Natural gas, a fossil fuel which is a mixture of several hydrocarbons, comprises mainly of methane ($CH_4$). In 2020, 37.1% of energy demand was fulfilled by natural gas in Canada.[2] Technological advancements have been made such that unconventional natural gas, such as shale gas, tight gas, and coalbed methane, has become more economically feasible; but despite these advancements, this fossil fuel remains a finite resource. Natural gas is a relatively clean burning fossil fuel compared to fossil fuels like coal and crude oil,[3] and as such still has value, even as energy sources transition to the renewable ones.[4] Furthermore, worldwide energy demands continue to increase,[1] so alternative energy sources must be investigated.

Methane is a greenhouse gas, with a global warming potential 25 times larger than that of $CO_2$ over the course of a century.[5] Of the 59 Gt $CO_2$ eq. total anthropogenic GHG emitted globally in 2019, 18% was due to methane.[1] Thus, a target for the mitigation of climate change are these methane emissions, which come from activities including agriculture, energy, wastewater and solid waste.[6]

The burning of fossil fuels results in the emission of flue gases, which typically comprises of species such as $N_2$, $CO_2$, $H_2O$, $O_2$, $NO_x$, $SO_x$, and CO.[7,8] It is thus vital to capture the greenhouse gases in these flue gases.

## 1.2 Post-Combustion Flue Gases

Combustion of fossil fuels like natural gas results in greenhouse gas emissions. Anthropogenic greenhouse gas emission is the primary cause of global warming. Therefore, the reduction of these emissions is a topic of interest for the mitigation of climate change. The main components of flue gas are $N_2$ (73-77%), $CO_2$ (15-16%), $H_2O$ vapour (5-7%), and $O_2$ (3-4%), with $NO_x$, $SO_x$, and CO in ppm levels.[7,9] As can be seen, $N_2$ and $CO_2$ are the gases in the largest quantity in this gas mixture. For this reason, studying binary mixtures of $N_2$ and $CO_2$ will be a large focus in this thesis.

Carbon dioxide is a greenhouse gas that comprises the majority of anthropogenic greenhouse gas emissions.[10] Carbon capture and storage, as well as carbon capture and utilization, are technologies which aim to reduce $CO_2$ emissions. Adsorption is one of such technologies on the carbon capture side, which will be examined in further detail in this work.

## 1.3 Adsorption

Adsorption is a surface phenomenon where atoms or molecules interact with a surface. The surface is referred to as the adsorbent and the atoms or molecules being adsorbed are referred to as the adsorbate. Adsorption can be classified into two categories: chemisorption and physisorption, where chemisorption involves a chemical bond forming between the adsorbent and the adsorbate and where physisorption involves weak van der Waals forces between the two. Physisorption is easily reversible, in contrast with chemisorption which is not practically reversible. The heat of adsorption can indicate whether physical adsorption or chemisorption is occurring; for physical adsorption, values are around 40 – 60 kJ/mol.[12]

In physisorption, or physical adsorption, van der Waals, which are always present, and electrostatic interactions, which are only significant in adsorbent with an ionic structure, between the adsorbate and the adsorbent are involved. The contribution of electrostatic interactions can result in a high heat of adsorption.[13]

## 1.4 Adsorbate Gases

The main focus in this thesis are $CO_2$, $CH_4$, $N_2$, and $O_2$. The properties of these gases are summarized in Table 1.1. Due to the higher quadrupole moment of $CO_2$, it is more strongly adsorbed than $CH_4$ and $N_2$. $CH_4$ will be adsorbed more strongly than $N_2$.

**Table 1.1** Properties of $CO_2$, $CH_4$, $N_2$, and $O_2$[14,15]

| Gas | Kinetic diameter (Å) | Polarizability ($x10^{-23}$ $cm^3$) | Dipole moment ($x10^{18}$ esu cm) | Quadrupole moment ($x10^{-26}$ esu $cm^2$) |
|---|---|---|---|---|
| $N_2$ | 3.64 | 17.6 | 0 | 1.52 |
| $O_2$ | 3.467 | 16.0 | 0 | 0.39 |
| $CH_4$ | 3.82 | 26.0 | 0 | 0 |
| $CO_2$ | 3.3 | 26.5 | 0 | 4.30 |

Kinetic adsorption processes, which can be done using molecular sieves adsorbents, separate species based on their kinetic diameter. However, the affinity of an adsorbate to the adsorbent surface due to aforementioned properties such as polarizability also have an effect in kinetic separation processes.

## 1.5 Adsorbents

A variety of commercially available adsorbents exist, such as carbon molecular sieves, activated carbons, metal organic frameworks (MOF), silica, and zeolites. In this project, commercially available activated carbons and carbon molecular sieves were studied. While a large amount of work has been done to characterize these types of adsorbents in terms of pure component adsorption capacities, gas mixture adsorption equilibrium measurements are less abundant. Experimental gas mixture data is more representative of industrial applications, where mixtures may not behave ideally, and thus is harder to model theoretically.

The performance of adsorbents can be measured based on several factors, including adsorption capacity, selectivity, kinetics, cost, and ease of regeneration. It is difficult to find an

adsorbent excelling at all these factors. Thus, design of an adsorption process requires the optimization of all these criteria.

### 1.5.1 Activated Carbons

Activated carbons are made from various carbon sources such as coal, coconut shells, and wood. Following raw material preparation, the manufacturing process first requires carbonization, followed by an activation step. Activation can be done chemically or by using a gas. Carbonization is done at a lower temperature, around 400 – 500°C, followed by activation at 800 – 1000 °C in the presence of an oxidizing gas to develop more uniform pores and increase the surface area. Chemical activation does not require a separate carbonization step and can vary depending on the activator compounds added to the raw material. The raw material and the activators are mixed together and carbonized at 500 – 900°C.[16]

Activated carbons are known to have a large surface area with a wide pore size distribution compared to other adsorbents. The surface is typically nonpolar, leading to hydrophobic properties,[13] meaning that pre-treatment of moisture need not be as strict as for hydrophilic adsorbents. They also adsorb more nonpolar molecules than other adsorbents, as well as typically having lower heats of adsorption.

### 1.5.2 Carbon Molecular Sieves

Carbon molecular sieves (CMS) are adsorbents with a narrow pore size distribution, similar to zeolites. The pore size can be tailored during the manufacturing process, allowing separation between molecules of similar size. For example, it is the adsorbent that can be used in the kinetic separation of $N_2$ and $O_2$.[14] As can be seen from Table 1.1, the kinetic diameter of $CH_4$ is larger than that of $CO_2$, $N_2$, and $O_2$, meaning separation by size exclusion is a topic of interest for certain applications. However, as mentioned above, other factors aside from kinetic diameter can affect the adsorption performance.

There are various methods of manufacturing CMS, which can vary by company, but many follow a similar general procedure. First, a carbon material such as coal is oxidized, then a carbonization step follows.[16,17]

## 1.6 Thesis Objectives

The main objective of this thesis was to screen adsorbents for use in the separation of $CH_4$ from $CO_2$ and $N_2$. To achieve that, some sub-objectives were also established. First, a reliable and accurate method for measuring pure component isotherms was sought by using concentration pulse chromatography. Second, pure component isotherms for various adsorbents were to be collected. Finally, binary isotherm data which would reflect gas mixture performance was to be obtained.

## 1.7 References


[1] Intergovernmental Panel on Climate Change, *AR6 Climate Change 2022: Mitigation of Climate Change*, P. R. Shukla, J. Skea, R. Slade, A. Al Khourdajie, R. van Diemen, D. McCollum, M. Pathak, S. Some, P. Vyas, R. Fradera, M. Belkacemi, A. Hasija, G. Lisboa, S. Luz, J. Malley, Eds., Cambridge University Press, Cambridge, UK, **2022**.

[2] Statistics Canada, Energy: Supply and demand, 2020. *Dly.* **2021**.

[3] S. Faramawy, T. Zaki, A. A. E. Sakr, *J. Nat. Gas Sci. Eng.* **2016**, *34*, 34.

[4] S. F. Ahmed, M. Mofijur, K. Tarannum, A. T. Chowdhury, N. Rafa, S. Nuzhat, P. S. Kumar, D. V. N. Vo, E. Lichtfouse, T. M. I. Mahlia, *Environ. Chem. Lett.* **2021**, *19*, 4137.

[5] Environmental Protection Agency, Inventory of U.S. Greenhouse Gas Emissions and Sinks: 1990-2018, **2020**, https://www.epa.gov/ghgemissions/inventory-us-greenhouse-gas-emissions-and-sinks-1990-2018.

[6] M. Saunois, A. R. Stavert, B. Poulter, P. Bousquet, J. G. Canadell, R. B. Jackson, P. A. Raymond, E. J. Dlugokencky, S. Houweling, P. K. Patra, P. Ciais, V. K. Arora, D. Bastviken, P. Bergamaschi, D. R. Blake, G. Brailsford, L. Bruhwiler, K. M. Carlson, M. Carrol, ..., Q. Zhuang, *Earth Syst. Sci. Data* **2020**, *12*, 1561.

[7] D. M. D'Alessandro, B. Smit, J. R. Long, *Angew. Chemie - Int. Ed.* **2010**, *49*, 6058.

[8] K. Sumida, D. L. Rogow, J. A. Mason, T. M. McDonald, E. D. Bloch, Z. R. Herm, T. H. Bae, J. R. Long, *Chem. Rev.* **2012**, *112*, 724.

[9] D. Saha, M. J. Kienbaum, *Microporous Mesoporous Mater.* **2019**, *287*, 29.

[10] J. Godin, W. Liu, S. Ren, C. C. Xu, *J. Environ. Chem. Eng.* **2021**, *9*, 105644.

[11] S. A. Rackley, *Carbon Capture and Storage*, 2nd ed., Butterworth-Heinemann, Oxford, **2017**.

[12] R. T. Yang, *Gas Separation by Adsorption Processes*, Butterworth, Stoneham, MA, **1987**.

[13] D. M. Ruthven, *Principles of Adsorption and Adsorption Processes*, John Wiley & Sons, New York, **1984**.

[14] S. Sircar, *Ind. Eng. Chem. Res.* **2006**, *45*, 5435.

[15] A. F. Ismail, K. C. Khulbe, T. Matsuura, *Gas Separation Membranes: Polymeric and Inorganic*, Springer International Publishing, **2015**.

[16] R. T. Yang, *Adsorbents: Fundamentals and Applications*, John Wiley & Sons, Hoboken, NJ, **2003**.

[17] A. L. Cabrera, J. E. Zehner, C. G. Coe, T. R. Gaffney, T. S. Farris, J. N. Armor, *Carbon N. Y.* **1993**, *31*, 969.

# Chapter 2 - Determination of adsorption isotherms using concentration pulse chromatography

**Dana Li**, Connor Francis, F. Handan Tezel

Department of Chemical and Biological Engineering, University of Ottawa

*161 Louis-Pasteur, Ottawa, Ontario, K1N 6N5 Canada*

## Abstract

Equilibrium adsorption isotherms of $CH_4$ with activated carbon were determined at 27$^oC$ using both a micro-gravimetric system as well as concentration pulse chromatography technique. The long column assumption for the determination of the slope of the isotherm from concentration pulse chromatography was verified experimentally by testing three column lengths in the gas chromatograph. The gravimetric and chromatographic adsorption isotherms up to 1 atm total pressure were comparable using all columns, but at higher pressures only the longest column's isotherm was similar to the adsorption capacity of $CH_4$ from the micro-gravimetric system. The flowrate used for concentration pulse chromatography was not observed to affect the isotherm slope measurement. This demonstrated the importance of column length in concentration pulse chromatography when measuring pure component isotherms, especially at high pressures.

**Keywords**

Gas adsorption, methane, activated carbon, concentration pulse chromatography

## 2.1 Introduction

There are multiple methods of measuring gas adsorption isotherms, including gravimetric technique, volumetric technique, and chromatographic technique. Various chromatographic techniques have previously been studied for the determination of pure component adsorption isotherms.[1–7] These include frontal analysis, elution technique, perturbation technique, and inverse chromatography. The perturbation technique, also called concentration pulse chromatography, involves analysis of the response peak from a small sample pulse to obtain the retention time at adsorption equilibrium. This retention time is used to find apparent equilibrium constants, which is then used to find the slopes of the isotherm.

Chromatographic techniques can apply both to the determination of single-gas adsorption isotherms, as well as binary gas mixture adsorption isotherms. For the determination of a single-gas isotherm, a mixture of known concentration of the target adsorbate gas and a non-adsorbed gas is used. The theory used for single-gas isotherm measurement can be extended to binary isotherm measurement.[8–13]

It is common to measure adsorption isotherms with a gravimetric or volumetric system. However, compared to the gravimetric or the volumetric system, chromatographic techniques only requires a gas chromatograph – a piece of equipment, which is relatively inexpensive and may already be owned in a research laboratory. This convenience makes the technique suitable for the determination of adsorption isotherms if more conventional methods are not available.

The use of concentration pulse chromatography for measuring pure component gas adsorption isotherms has been carried out in the past,[6, 7, 10, 11] so one of the goals of this study was to experimentally confirm the assumption of a sufficiently long adsorption column made in this method. Another purpose of this study was to obtain pure component gas adsorption isotherm for $CH_4$ with an activated carbon from 0 to 7 atm total pressure at room temperature (27˚C) using concentration pulse chromatography. The accuracy of the adsorption isotherm from concentration pulse chromatography was compared with the results obtained from the gravimetric analysis, a more common method of measuring adsorption isotherms.

## 2.2 Materials and Methods

### 2.2.1 Material

Activated carbon sample labeled AC-C was provided by Xebec Adsorption Inc. (Blainville, Quebec, Canada). The activated carbon pellets were crushed to 50x70 US mesh (210-297 μm) size. Gas cylinders of He (99.999%) and $CH_4$ (99.99%) were purchased from Messer Canada Inc. (Ottawa, Ontario, Canada).

### 2.2.2 Concentration Pulse Chromatography

A modified GOW-MAC (Bethlehem, Pennsylvania, USA) Series 400 gas chromatograph (GC) equipped with a thermal conductivity detector (TCD) was used to measure $CH_4$ isotherms on activated carbon. The experimental setup has been described in previous papers for use in determination of binary mixture isotherms[13,14] and its schematic diagram is shown in Figure 2.1. For pure component isotherms, the procedure is similar, but the most important difference between the two is the fact that for pure component isotherm determination, an inert gas (such as He) is used in the carrier gas mixed with the gas for which the isotherm is going to be determined. Gas components in the carrier gas are connected to individual mass flow controllers (MFC), allowing the manipulation of mixed carrier gas concentrations. The carrier gas passes through the reference side of the TCD before entering the six-port injection valve. After the injection of the sample gas in the six-port injection valve, it passes through the adsorption column and then through the sample side of the TCD and the bubble meter before it is vented into the fume hood. There are also back pressure resistance valves on the carrier gas and the sample gas sides, allowing the variation of total pressure inside the GC.

A packed column with an inner diameter of 0.46 cm was used in the gas chromatograph. Three different column lengths were tested: 3.4 cm, 8.7 cm, and 15 cm. A void fraction of 0.375 was determined by using glass beads of the same particle size as the crushed activated carbon in a graduated cylinder and with deionized water. The particle density was measured by packing a column with adsorbent, weighing the sample in the column, then using the void fraction to get a particle density of 811 kg $m^{-3}$. The dead volume retention time for the gas chromatograph was

determined with a packed column of glass beads, using a sample pulse of $N_2$ in a carrier gas of He with flowrate of 7 ccm.

After packing the adsorbent column with activated carbon, the adsorbent was regenerated inside the GC by flowing He as purge gas at an oven temperature of 150°C for 2 hours. Afterwards, the column was cooled to 27°C, which was as close to room temperature as could be controlled in the GC enclosure, while He continued to flow through the column. He was assumed to be not adsorbed appreciably.

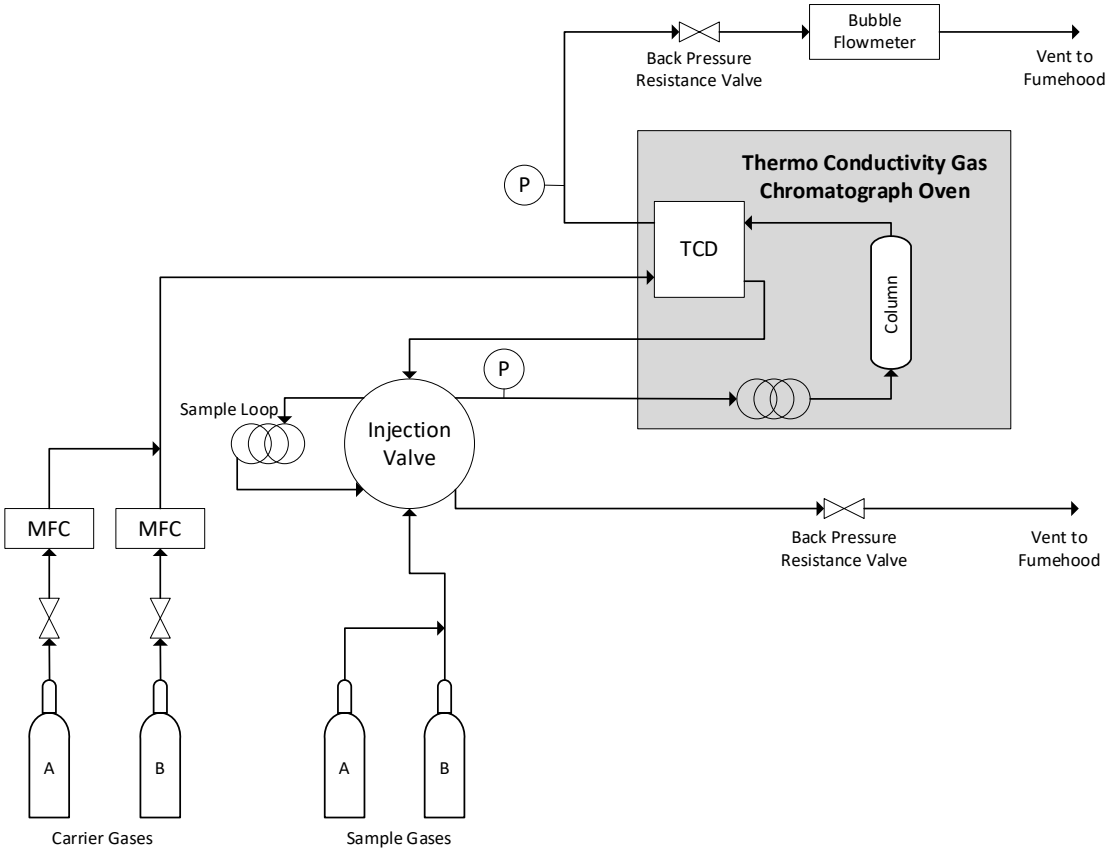


Figure 2.1 Schematic diagram of the modified GOW-MAC GC used in this study for the determination of pure component adsorption isotherms.

For the determination of pure component adsorption isotherms, a mixture of He and $CH_4$ was used in the carrier gas with total carrier gas flowrates at their respective pressures given in Table 2.1. Flowrates were decided based on having reasonable residence times that were neither too short to measure, nor too long in which case potential baseline could drift over time. For the

3.4 cm column, a mass flow controller with a maximum flow-rate of 10 sccm was used, which limited the volumetric flowrate at higher pressures. For the 15 cm column, a mass flow controller with a limit of 100 sccm was used at high pressures because the residence time in the column was significantly longer due to increased column length. To vary the partial pressure of $CH_4$ in the system, flow rates of $CH_4$ and He gases were controlled with mass flow controllers at a constant total pressure in the GC column. $CH_4$ was used as the sample gas injected, and the response of the adsorption column was monitored as concentration of $CH_4$ as a function of time at the outlet of the column. The resulting peak obtained can then be integrated to obtain the mean retention time, $\mu$, at a certain partial pressure of $CH_4$ in the carrier gas. From the mean retention time, the apparent equilibrium constant, $K$ was calculated by using Eq. (2.1).[8]

Table 2.1 Total carrier gas flowrates (in ccm) for concentration pulse chromatography experiments with 3.4 cm, 8.7 cm, and 15 cm columns at 1, 4, and 7 atm total pressures.

| **Total pressure (atm)** | **Column length (cm)** | | |
|---|---|---|---|
| | 3.4 | 8.7 | 15 |
| | **Volumetric flowrate (ccm)** | | |
| 1 | 7.0 | 7.0 | 7.0 |
| 4 | - | 7.0 | 7.0 |
| 7 | 1.4 | 1.4 | 7.0 |

$$\mu = \frac{\int_0^\infty c(t-\mu_d)dt}{\int_0^\infty c\,dt} = \frac{L}{v}\left[1 + \frac{(1-\varepsilon)K}{\varepsilon}\right] \tag{2.1}$$

Where $c$ is the concentration, $t$ is time, $\mu_d$ is the dead volume retention time, $L$ is the column length, $v$ is the interstitial carrier gas velocity, and $\varepsilon$ is the bed void fraction. The dead volume retention time represents the time required for the sample gas to travel through piping in the system, excluding the length of the column, and to reach the GC detector; this value must be used when calculating the mean residence time corrected for the dead volume, $\mu_d$.

The right-most side of Eq. (2.1) comes from the mass balance on the column. To simplify the mass balance, it was assumed that the column is infinitely long and that there is no pressure drop in the column.[15]

The dimensionless $K$ is related to the dimensional equilibrium constant, $K_p$, by the gas constant, $R$, the temperature, $T$, and the particle density, $\rho_p$ (Eq. (2.2)).

$$K_p = \frac{K}{RT\rho_p} \tag{2.2}$$

In order to measure adsorption using concentration pulse chromatography, the adsorbate must diffuse into the adsorbent micropores. If there is only negligible diffusivity, then the chromatographic peak will only reflect the dead volume.[16] The second moment of the response peak is dependent on mass transfer characteristics which include the axial dispersion, the molecular diffusion, the macropore diffusion, and the micropore diffusion. The contribution of the molecular diffusion, macropore diffusion, and micropore diffusion to the mass transfer resistance should be greater than the axial dispersion,[17,18] which requires a long column and smaller flowrates.[16,19] Another experimental condition for reliable values from the chromatographic method is that K>>1.0.[15] In this study, the temperature was 27°C and the particle density was 811 kg $m^{-3}$, meaning that $K_p$>>0.050 mol $kg^{-1}$ $atm^{-1}$ should be measured for reliable results.

In a binary gas mixture adsorption case, both components in the mixture contribute to the overall $K_p$ value, since they are both adsorbed. This can be expressed mathematically by Eq. (2.3), where $y_1$ is the mole fraction of component 1 in the gas phase, and $dq_i/dP_i$ is the slope of the isotherm for component $i$ in the mixture at the corresponding value of $y_1$.[9] The more strongly adsorbed component can be written as component 1, and the less strongly adsorbed component as component 2. In this study, $CH_4$ was considered as component 1 and He as component 2. It can be seen that at low $y_1$ values, the contribution of component 2 to the overall $K_p$ value is negligible. As $y_1 \rightarrow 1$, the consideration of the slope of component 2 becomes significant and should not be neglected.[8] Since He was assumed to not be adsorbed appreciably, the slope of the He isotherm was taken to be a constant, $E$, as shown in Eq. (2.4). The value of $E$ was found by curve fitting the $K_p$ vs $y_1$ data for each total pressure and extrapolating the data to $y_1 \rightarrow 1$.[6,7] $E$ was found to be greater at 1 atm total pressure than at 4 atm and 7 atm, but in the same order of magnitude. As such, slopes at a given total pressure were calculated with Eq. (2.4) using $E$ from that total pressure.

$$K_p = (1 - y_1)\frac{dq_1}{dP_1} + y_1\frac{dq_2}{dP_2} \quad (2.3)$$

$$K_p = (1 - y_1)\frac{dq_1}{dP_1} + y_1 E \quad (2.4)$$

Once $K_p$ is determined at different partial pressures of $CH_4$, these experimental slopes of the isotherm can then be integrated to obtain the pure component adsorption isotherm of $CH_4$.

In this study, total pressures of 1 atm, 4 atm, and 7 atm were considered at 27°C, while the mole fractions of He and $CH_4$ in the carrier gas were changed in order to conduct experiments at different partial pressures of $CH_4$, up to the partial pressure of 6.3 atm for $CH_4$.

### 2.2.3 Gravimetric Analysis

A Hiden-Isochema (Warrington, Cheshire, United Kingdom) IGA-003 gravimetric analyzer was used to measure $CH_4$ isotherm on activated carbon. After loading the sample into the sample holder, the adsorbent was regenerated at 150°C under vacuum for 2 hours. A helium gas adsorption isotherm was used to measure the skeletal density to correct for buoyancy during experiments at high pressures. The pure gas adsorption isotherm of $CH_4$ was then determined at 27°C to compare with the results obtained from the concentration pulse chromatography.

### 2.2.4 Isotherm Model

Various models exist to describe pure component gas adsorption isotherm behaviour, expressing the adsorption capacity $q$ as a function of pressure $P$. The Langmuir[20] and Sips[21] isotherm models were used to fit the experimental data. It was found that the Sips model shown in Eq. (2.5) fit the data the best, so only Sips will be described in detail. This model resembles the Langmuir model, where the adsorbent eventually becomes saturated at limiting adsorption capacity, $q_m$, as P approaches infinity. The equilibrium constant $B$ can be approximated by the initial slope of the isotherm. However, unlike the Langmuir model, the Sips model does not assume that each adsorbed molecule occupies one adsorption site. Instead, a molecule is assumed to occupy $n$ number of adsorption sites.

$$q = \frac{q_m (BP)^{1/n}}{1 + (BP)^{1/n}} \tag{2.5}$$

## 2.3 Results and Discussion

### 2.3.1 Concentration Pulse Chromatography

To investigate the effect of adsorbent column length on accuracy of the pure component gas adsorption isotherm, three columns of different lengths were used. This was to ensure that the infinitely long column assumption in the mass balance was reflected in the experimental analysis.

The $K_p$ values, as well as the $CH_4$ isotherm slopes, determined as a function of the partial pressure of $CH_4$, for all columns at 27°C for 1, 4, and 7 atm total pressures are shown in Figure 2.2. All $K_p$ values were higher than 0.050 mol $kg^{-1}$ $atm^{-1}$, which was one of the conditions mentioned above for reliable concentration pulse chromatography measurements. The two figures are similar, but it visually shows the importance of converting $K_p$ into the isotherm slope at high mole fractions of $CH_4$. Furthermore, the slope of the He adsorption isotherm, *E*, was found to be important for correcting the $CH_4$ isotherm slope especially at high mole fractions of $CH_4$. Isotherm slopes for $CH_4$ were calculated from $K_p$ using *E* that corresponded to the total pressure used and are shown in Table 2.2.

Table 2.2 He slope, *E*, measured at 1, 4, and 7 atm total pressure with 3.4, 8.7, and 15 cm columns

| **Total pressure (atm)** | **Column length (cm)** | | |
|---|---|---|---|
| | 3.4 | 8.7 | 15 |
| | **He slope (mol $kg^{-1}$ $atm^{-1}$)** | | |
| 1 | 0.210 | 0 | 0.0685 |
| 4 | - | 0.0345 | 0.0255 |
| 7 | 0.840 | 0.294 | 0.0291 |

It was observed that *E* varied depending on the total pressure. Based on the assumption that the He isotherm slope is constant, this should not have been the case. However, this could be attributed to experimental error. For example, the uncertainty in the $K_p$ measurement increased as $P_{CH_4}$ approached the total pressure for each curve shown in Figure 2.3.

For the 15 cm column, the value of $E$ generally decreased as the total pressure increased, which could be due the He slope decreasing slightly with increasing pressure, despite assumptions that the He slope is constant. As for the values of $E$ for the 3.4 cm and 8.7 cm columns, $E$ increased as total pressure increased. As will be discussed with the $CH_4$ isotherm slope with respect to the column length and can be seen in Figure 2.2, it was found that the 3.4 cm and 8.7 cm columns overestimated the $CH_4$ slope at pressures above atmospheric. The same was seen in the He slope for the 3.4 cm and 8.7 cm columns at 7 atm. To reduce error associated with $E$, the data points at high $y_{CH_4}$ were omitted from the overall isotherm averaging all data collected because these data points are affected more by $E$, as shown in Eq. (2.4).

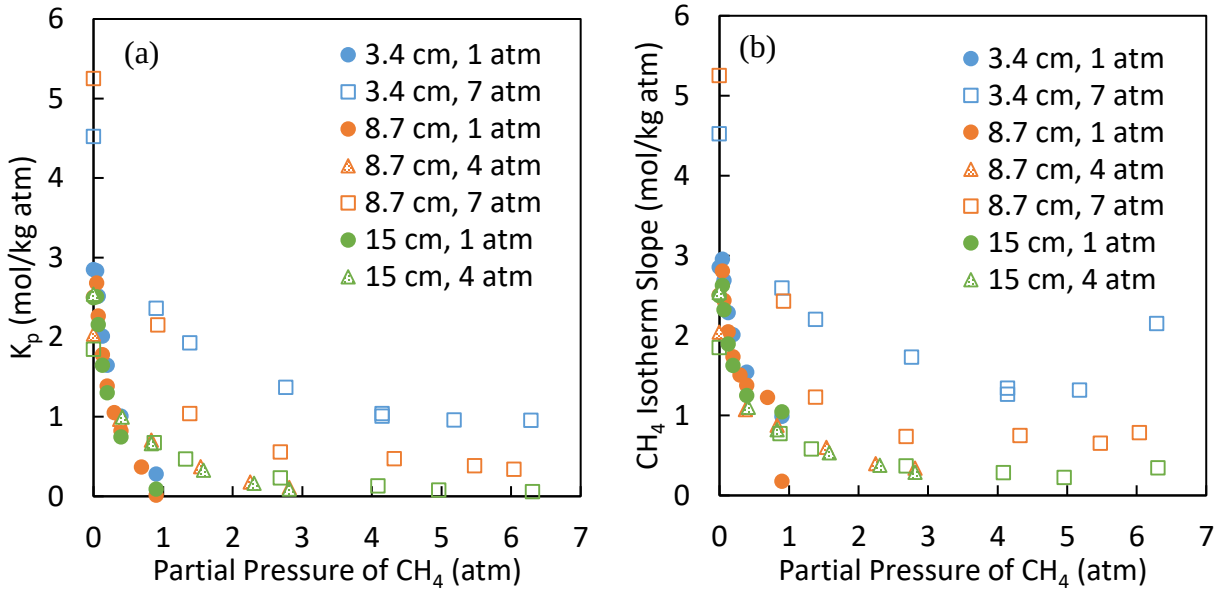


Figure 2.2 (a) $K_p$ vs partial pressure of $CH_4$ and (b) $CH_4$ isotherm slope vs partial pressure of $CH_4$ for 3.4 cm, 8.7 cm, and 15 cm long columns at 27°C using AC-C at 1, 4, and 7 atm total pressures.

When the $K_p$ values collected at 1 atm total pressure for the three different column sizes are compared, it could be seen that all data coincide (shown as circles in Figure 2.2). This was expected since the $K_p$ value at a given partial pressure of $CH_4$ should not change as the column length changed, if the column was sufficiently long.

The data collected at 4 atm total pressure for the different columns also overlap with each other (shown as triangles in Figure 2.2). It also agreed with the 1 atm total pressure data at partial

pressures of $CH_4$ ($P_{CH_4}$) lower than 0.4 atm. However, at $P_{CH_4}$ of 0.9 atm, the $K_p$ at 4 atm total pressure was 0.68 mol $kg^{-1}$ $atm^{-1}$, while at 1 atm total pressure it was 0.098 mol $kg^{-1}$ $atm^{-1}$ on average. Even when comparing the isotherm slopes at these conditions, there was a large difference especially for the 8.7 cm column.

The effect of column length was even more evident at 7 atm total pressure. $K_p$ measured with the 3.4 cm column was much higher than with the 15 cm column. This was also seen in the isotherm slope as a function of $P_{CH_4}$.

While the data collected at 1, 4, and 7 atm total pressure on the 15 cm column formed a continuously decreasing curve, the same was not seen for the data on the 3.4 cm and 8.7 cm columns. Observing the blue circles in Figure 2.2 (b), data from the 3.4 cm column at 1 atm total pressure, it can be seen that the $CH_4$ isotherm slope decreases with $P_{CH_4}$ as expected. Then, comparing the blue circles to the blue squares in Figure 2.2 (b), data from the 3.4 cm column at 7 atm total pressure, there is a jump in the data around $P_{CH_4}$ = 0.9 atm. A similar occurrence can be seen in the data collected with the 8.7 cm column, shown in orange points, where the measured $CH_4$ isotherm slope value jumps as the total pressure changes. The jumps between data collected at 1 atm total pressure and 7 atm total pressure was the greatest for the 3.4 cm column. Since the slope of the pure component $CH_4$ isotherm should only depend on the partial pressure of $CH_4$ and not the total pressure, the data collected with the 3.4 cm and 8.7 cm columns were not considered accurate, since the infinitely long column assumption for the derivation of the equations would not be valid for these shorter columns. This aligns with the fact that there is a higher possibility of correctly measuring a chromatographic peak when using a longer column. For this reason, the 15 cm column was taken to be the most accurate data collected in these experiments. Using a shorter column resulted in an overestimation of the actual adsorption capacity.

The necessity for the use of a sufficiently long column comes out of the assumptions made to obtain Eq. (2.1). The mass balance assumes that the packed column is sufficiently long. As observed in these experiments, erroneous results may be obtained when the column is too short.

Furthermore, it was observed that data was less reliable at high molar fractions of adsorbate ($CH_4$ in this case) in the carrier gas, which is shown in the percentage correction for mean residence times in Figure 2.3. Percentage $\mu$ correction was calculated by taking the ratio of $\mu_d$, the dead volume time, over the raw value of the mean residence time, or $\mu_{raw}$ (uncorrected for $\mu_d$). At high mole fractions of $CH_4$, the mean residence time decreased, thus the $K_p$ value decreased. This is

expected, since isotherm slope decreases at higher pressures for favorable isotherms. At lower $K_p$ values, where we would have high concentrations of $CH_4$, the dead time correction becomes much more significant. It can be seen that corrections of over 50% of the mean residence time were made, especially at higher total pressures and higher mole fractions of $CH_4$. At 1 atm total pressure, the 3.4 cm column had the largest percentage correction for $\mu_{raw}$, whereas the 15 cm column had the lowest. A similar trend was seen at 4 atm total pressure, where the 15 cm column had lower corrections for $\mu_{raw}$ compared to the 8.7 cm column. However, at 7 atm total pressure, it was seen that the $\mu_{raw}$ corrections were the highest for the 15 cm column. Due to using a higher flowrate with the 15 cm column at 7 atm total pressure (7 ccm) to collect data at a reasonable speed, the $\mu_{raw}$ with the 15 cm column were smaller than with the other columns, resulting in the $\mu_{raw}$ correction to account for a larger percentage of the actual value.

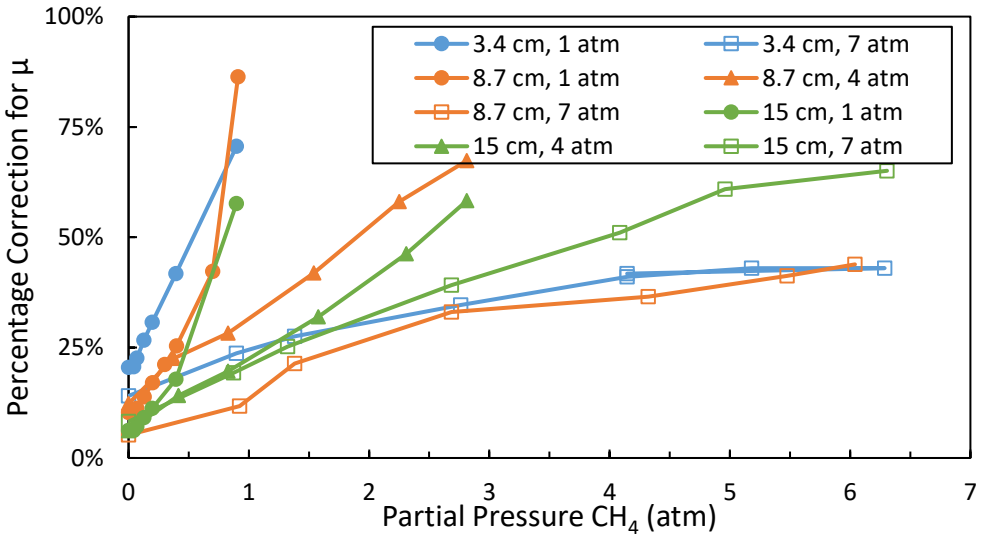


Figure 2.3 Percentage $\mu$ correction for $CH_4$ mean residence time in 3.4 cm, 8.7 cm, and 15 cm columns at 27°C using AC-C.

The $CH_4$ isotherms plotted for the 3.4 cm, 8.7 cm, and 15 cm columns are plotted separately in Figure 2.4. The resulting isotherms for data within the same total pressure are plotted, along with the overall isotherm using data from all total pressures. For the 3.4 cm column, it could be seen that the isotherm using only data collected at 7 atm total pressure showed $CH_4$ adsorption capacity larger than the isotherm using only data collected at 1 atm total pressure. This was also

observed in the $K_p$ - $P_{CH_4}$ data, since $K_p$ was used to obtain the isotherm slope, which was integrated to obtain the adsorption isotherm. A similar trend was seen with the data collected on the 8.7 cm column, where the adsorption capacity in the isotherm using only data collected at 7 atm total pressure was much higher than those collected at 1 atm or 4 atm total pressure. For the 8.7 cm column, it was seen that the isotherm using only data at 1 atm and the isotherm using only data at 4 atm total pressure appeared continuous with each other. This is the result that was expected of accurate data - that the total pressure would not have an effect on the measured isotherm slope.

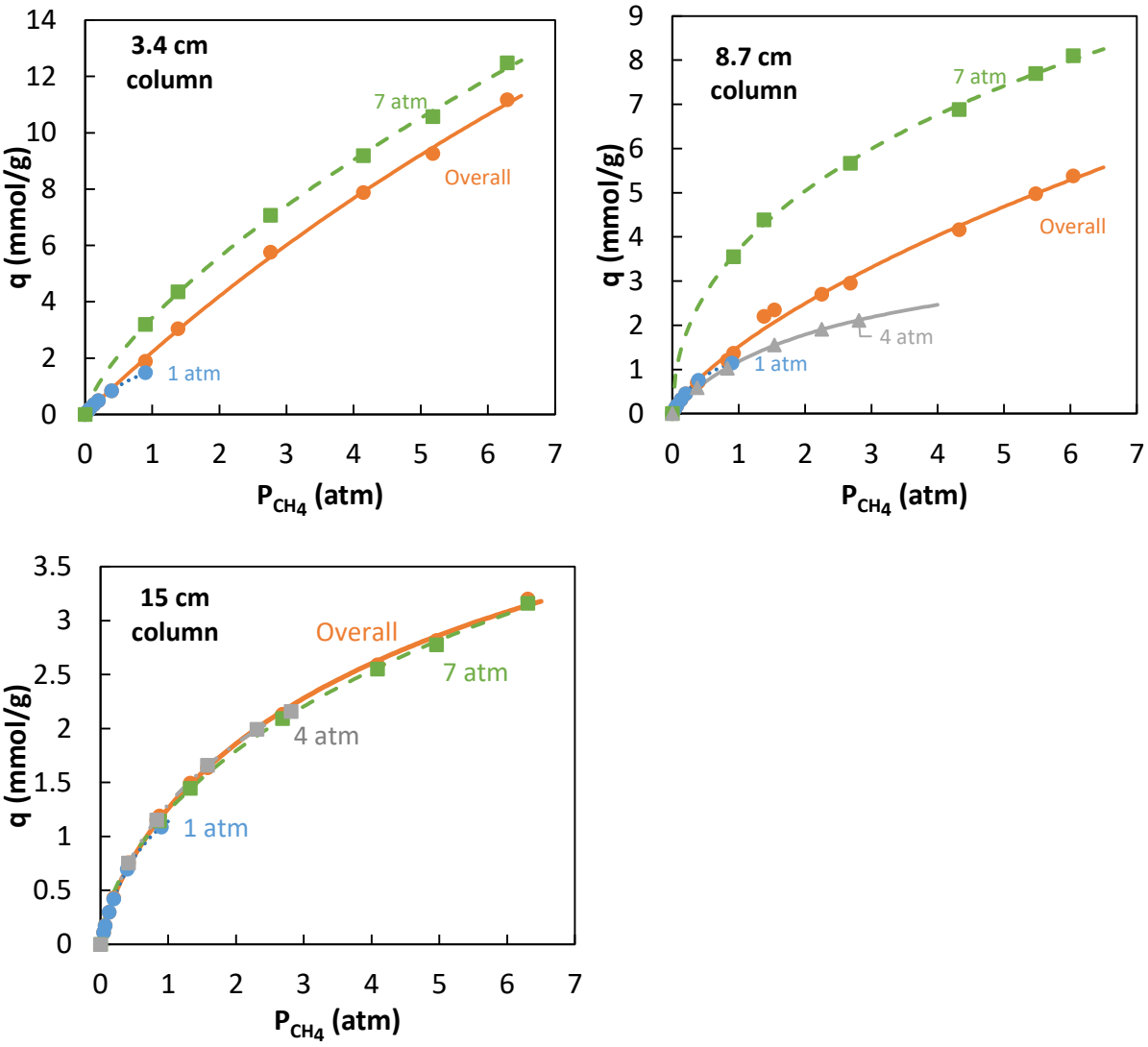


Figure 2.4 $CH_4$ isotherm from concentration pulse chromatography on AC-C at 27°C using 3.4 cm, 8.7 cm, and 15 cm column, with Sips model fit curve at 1 atm, 4 atm, and 7 atm total pressures, and overall using data collected at all total pressures.

Data at 4 atm total pressure was not collected with the 3.4 cm column, so only data at 1 atm and 7 atm total pressure were used to calculate its overall $CH_4$ isotherm. Data at 1, 4, and 7 atm total pressure were collected with the 8.7 cm column, so the adsorption capacities in the overall isotherm were closer to the isotherms using only data at 1 atm or 4 atm rather than at 7 atm. Both overall isotherms collected with the 3.4 cm column and the 8.7 cm column were not very accurate, however, as there was a clear overestimation of adsorption capacity at 7 atm total pressure.

For the 15 cm column, like with the $K_p$ values, it could be seen that there was agreement between the data collected at 1 atm, 4 atm, and 7 atm total pressure when partial pressure of $CH_4$ is low (less than 0.4 atm).

The overall isotherm was taken to be the experimental isotherm determined with concentration pulse chromatography, using data collected with the 15 cm column at all total pressures. As mentioned above, $E$ only affects the isotherm slope considerably at high $y_{CH_4}$. To reduce the error introduced at high $y_{CH_4}$ due to dead time correction and $E$ correction, data points at 1 atm and 4 atm total pressure were excluded from the overall isotherm. Data was excluded when effect of $E$ was noticeable, which was determined with results in Figure 2.2 (b), when $K_p$ did not make a continuous curve. At 1 atm total pressure, points at $P_{CH_4}$=0.4 and 0.9 atm were omitted and at 4 atm total pressure, points at $P_{CH_4}$= 2.3, 2.8 atm were omitted. These are experimental points where there is greater uncertainty in the measurement due to the sample gas composition approaching that of the reference gas at the thermal conductivity detector, and the $K$ values approach 0.

Table 2.3 Sips parameters for $CH_4$ isotherm on AC-C at 27°C obtained with concentration pulse chromatography and with micro-gravimetric system.

| | **Sips Parameters** | | | |
|---|---|---|---|---|
| | B | $q_0$ | n | SSR |
| | $atm^{-1}$ | mmol $g^{-1}$ | - | mmol $g^{-1}$ |
| CPC | 0.1419 | 6.5544 | 1.3600 | 1.35E-02 |
| Gravimetric | 0.2028 | 5.7067 | 1.2093 | 1.52E-03 |

The overall $CH_4$ isotherm was fitted with the Langmuir and Sips models, and the Sips coefficients of the isotherm model can be found in Table 2.3. While the Langmuir model provided a reasonable fit for the data, it was found that the Sips model represented the data better.

### 2.3.2 Comparison of Chromatographic and Gravimetric Results

The $CH_4$ isotherm obtained for AC-C gravimetrically at 27°C is shown in Figure 2.5, plotted alongside the overall isotherm obtained with concentration pulse chromatography at 27°C obtained with the 15 cm column. The gravimetric data was taken as the more reliable one, as it is a well established procedure. As can be seen, the gravimetric data and the CPC data showed agreement. As shown in Figure 2.3, the dead time correction accounted for a large percentage of correction, which could lead to some error with the CPC method. Nevertheless, the isotherm measured with CPC using a 15 cm long column was found to be accurate as it matched the isotherm measured gravimetrically.

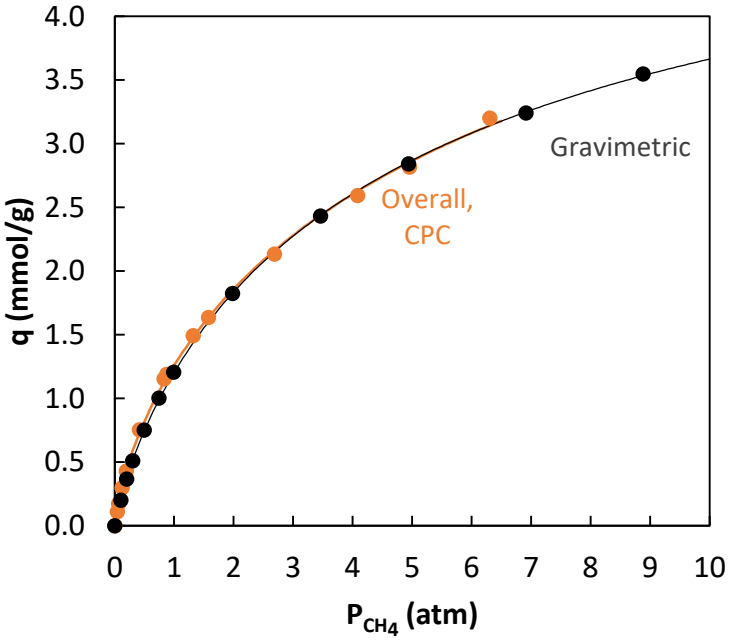


Figure 2.5 $CH_4$ isotherm on AC-C at 27°C with Sips model fit line for data from gravimetric system and from concentration pulse chromatography (CPC).

Comparing the gravimetric data to the isotherms on the 3.4 cm and the 8.7 cm column in Figure 2.4, it was clear that the two shorter columns tested in this study overestimated the $CH_4$

adsorption capacity at high pressures. These results indicate that to measure accurate isotherms with CPC, it is recommended to collect data at different total pressures and ensure that the isotherm slope does not change with respect to the total pressure (seen with the 3.4 cm and 8.7 cm column), and it changes only with the partial pressure of adsorbate (seen with the 15 cm column).

## 2.4 Conclusions

Concentration pulse chromatography was used to measure the adsorption isotherm of methane on activated carbon at 27°C by analyzing the retention time to get slope of the isotherm at different partial pressures of $CH_4$ in the carrier gas, which were then integrated to obtain the isotherm. The infinite column size assumption made in the mass balance for the concentration pulse chromatography method was verified by testing three different column lengths (3.4 cm, 8.7 cm, and 15 cm), and it was observed that a short column resulted in an overestimation of the isotherm slope at pressures above atmospheric.

Comparing the CPC isotherm data with the gravimetric isotherm data, it was found that there was good agreement between the two at partial pressures of $CH_4$ below 1 atm, but at higher pressures, it was found that the CPC data underestimated the $CH_4$ adsorption capacity on the two shorter columns. With the 15 cm column, CPC results at all partial pressures of $CH_4$ matched the gravimetric data well. Thus, a 15 cm column was found to be sufficiently long to comply with the infinite column assumption. The dead volume correction accounted for a large percentage of the measured retention time, leading to large uncertainties at high pressures. CPC can be used to measure pure component isotherms, which can be advantageous due to the inexpensive setup. In order for the CPC method to be used to measure pure component isotherms at high pressures, the column must be long enough that the isotherm slope varies only with the adsorbate partial pressure but not the total system pressure. Measurements at high mole fraction of adsorbate gases should be carried out, in order to estimate the value of $E$ to calculate the isotherm slope from $K_p$.

## 2.5 Nomenclature

| | |
|---|---|
| $B$ | Langmuir parameter ($atm^{-1}$) |
| $c$ | Concentration (mol $m^{-3}$) |

| | |
|---|---|
| $E$ | Slope of He isotherm (mmol $g^{-1}$ $atm^{-1}$) |
| $K$ | Apparent equilibrium constant (-) |
| $K_p$ | Dimensional apparent equilibrium constant (mmol $g^{-1}$ $atm^{-1}$) |
| $L$ | Column length (m) |
| $n$ | Sips parameter (-) |
| $P$ | Pressure (atm) |
| $P_{CH_4}$ | Partial pressure of methane (atm) |
| $P^0_i$ | Equilibrium pressure at the same adsorption capacity as the spreading pressure (atm) |
| $R$ | Gas constant ($m^3$ atm $K^{-1}$ $mol^{-1}$) |
| $q$ | Adsorption capacity (mmol $g^{-1}$) |
| $q_m$ | Limiting (maximum) amount adsorbed (mmol $g^{-1}$) |
| $t$ | Time (s) |
| $T$ | Temperature (K) |
| $v$ | Interstitial velocity (m $s^{-1}$) |
| $y_i$ | Mole fraction of component i in the gas phase (-) |

## Greek Letters

| | |
|---|---|
| $\varepsilon$ | Adsorbent bed porosity (-) |
| $\mu$ | Mean retention time (s) |
| $\mu_d$ | Dead volume time (s) |
| $\mu_{raw}$ | Raw mean retention time, not corrected for dead volume time (s) |
| $\rho_p$ | Particle density (kg $m^{-3}$) |

## Abbreviations

| | |
|---|---|
| AC | Activated carbon |
| CPC | Concentration pulse chromatography |
| GC | Gas chromatograph |
| MFC | Mass flow controller |
| SSR | Sum of square residuals |
| TCD | Thermal conductivity detector |

## 2.6 References


[1] P. J. Kipping, D. G. Winter, *Nature* **1965**, *205*, 1002.

[2] P. Valentin, G. Guiochon, *J. Chromatogr. Sci.* **1976**, *14*, 132.

[3] J. Å. Jönsson, P. Lövkvist, *J. Chromatogr.* **1987**, *408*, 1.

[4] S. H. Hyun, R. P. Danner, *AIChE J.* **1985**, *31*, 1077.

[5] F. Roubani-Kalantzopoulou, *J. Chromatogr. A* **2004**, *1037*, 191.

[6] F. H. Tezel, H. O. Tezel, D. M. Ruthven, *J. Colloid Interface Sci.* **1992**, *149*, 197.

[7] P. J. E. Harlick, F. H. Tezel, *Sep. Purif. Technol.* **2003**, *33*, 199.

[8] D. M. Ruthven, R. Kumar, *Ind. Eng. Chem. Fundam.* **1980**, *19*, 27.

[9] E. van der Vlist, J. van der Meijden, *J. Chromatogr.* **1973**, *79*, 1.

[10] R. W. Triebe, F. H. Tezel, *Can. J. Chem. Eng.* **1995**, *73*, 717.

[11] P. J. E. Harlick, F. H. Tezel, *Adsorption* **2000**, *6*, 293.

[12] P. Li, F. H. Tezel, *J. Chem. Eng. Data* **2008**, *53*, 2479.

[13] D. Kennedy, F. H. Tezel, *Adsorption* **2014**, *20*, 189.

[14] P. Li, F. H. Tezel, *Sep. Sci. Technol.* **2007**, *42*, 3131.

[15] J. Kärger, D. M. Ruthven, D. N. Theodorou, *Diffusion in Nanoporous Materials*, Wiley-VCH, Weinheim, Baden-Württemberg, **2012**.

[16] H. W. Habgood, W. R. Macdonald, *Anal. Chem.* **1970**, *42*, 543.

[17] T.-S. Chou, *Chem. Eng. Sci.* **1979**, *34*, 133.

[18] D. M. Ruthven, F. H. Tezel, J. S. Devgun, T. S. Sridhar, *Can. J. Chem. Eng.* **1984**, *62*, 526.

[19] N. S. Raghavan, D. M. Ruthven, *Chem. Eng. Sci.* **1985**, *40*, 699.

[20] I. Langmuir, *J. Am. Chem. Soc.* **1918**, *40*, 1361.

[21] R. Sips, *J. Chem. Phys.* **1948**, *16*, 490.

# Chapter 3 - Adsorbent screening for $CO_2$ capture by pure component isotherm measurements

**Dana Li**, F. Handan Tezel

Department of Chemical and Biological Engineering, University of Ottawa

*161 Louis-Pasteur, Ottawa, Ontario, K1N 6N5 Canada*

## Abstract

Experimental pure component isotherms of $CO_2$ and $N_2$ adsorption on commercially available carbon molecular sieves (CMS) and activated carbons (AC) were measured gravimetrically at 25°C. Additional isotherms at 16°C and 35°C were also measured for CMS's, as well as $O_2$ adsorption isotherms. $CO_2$ adsorption capacities were the highest among the gases studied. At 25°C, AC's were found to have greater adsorption capacities, with AC-B demonstrating the highest $CO_2$ adsorption capacities overall. Trends for CMS adsorption capacities and selectivity values varied depending on the temperature, which matched the trends in isosteric heats of adsorption showing very high heats of adsorption for CMS-A and CMS-C for $CO_2$. For adsorption at 25°C, the adsorbent with the highest $CO_2$ adsorption capacity and $CO_2/N_2$ selectivity values below 1.5 atm was AC-C, and above 1.5 atm it was AC-B. The samples tested had similar adsorption capacities and $CO_2/N_2$ selectivity values as other commercially available adsorbents in the literature. Using pure component adsorption model fits for the Langmuir model, the $CO_2$-$N_2$ binary mixture adsorption isotherms were predicted with the Extended Langmuir Model and the Ideal Adsorbed Solution Theory at 25°C and 1 atm total pressure for different compositions in the gas phase; the Flory-Huggins Vacancy Solution Theory was also used for prediction. At these conditions, AC-A had the highest $CO_2/N_2$ selectivity among all the adsorbents studied due to most of the adsorbents having similar $N_2$ adsorption capacities but different $CO_2$ adsorption capacities. At 1 atm AC-A had the highest $CO_2$ adsorption capacity. Among the CMS samples, CMS-B had the highest $CO_2$ adsorption capacity and $CO_2/N_2$ selectivity.

**Keywords**

Carbon dioxide adsorption, activated carbon, carbon molecular sieves

## 3.1 Introduction

$CO_2$ emissions released as a product of anthropogenic activity is the main contributor to greenhouse gases (GHG). As stated by the Intergovernmental Panel on Climate Change, it is an established fact that these human actions have an impact on the climate.[1] From 2010 to 2019, total anthropogenic GHG emissions increased by 1.3% per year, with 75% of emissions resulting from $CO_2$.[2]

To reduce the environmental impact of these activities, $CO_2$ separation is a topic of interest. It most often needs to be separated from $N_2$, as most $CO_2$ emissions occur as a result of fossil fuel usage. However, other instances where $CO_2$ separation is required include biogas upgrading, natural gas upgrading, syngas production and direct carbon capture.[3] Typical compositions of post combustion gases by volume is 73-77% $N_2$, 15-16% $CO_2$, 5-7% $H_2O$, 3-4% $O_2$, with $NO_x$, $SO_x$, and CO present in ppm levels.[4,5] The most common technology used for post combustion $CO_2$ capture is absorption, using amines like monoethanolamine. Despite the wide use of absorption in industry however, there are a number of disadvantages, such as energy intensive regeneration and solvent degradation sensitivity.[4]

Given that chemical absorption is an energy-intensive process, physical adsorption has been proposed as a process for $CO_2$ separation. Adsorbents can be selective for certain adsorbates either based on affinity to the adsorbent surface, or based on size exclusion. Size exclusion based separation occurs in molecular sieves, where the average pore size and size distribution is much smaller.[6] Some adsorbents used for $CO_2$ adsorption included activated carbon, carbon molecular sieves (CMS), silica, metal-organic framework materials, and zeolites. Carbon based adsorbents are of interest because they are more hydrophobic than zeolites, have high surface area, and surface modification is possible for tailoring their properties.[7] As for carbon molecular sieves, they are also more hydrophobic than zeolites, and their narrow pore size distribution allows preferential kinetic adsorption of $CH_4$ over $CO_2$.[8]

In this study, commercially available activated carbons and carbon molecular sieves were screened by measuring pure component $CO_2$ and $N_2$ gas adsorption isotherms using a gravimetric system up to 10 atm. pressure. Binary gas mixture adsorption isotherms were also predicted using theoretical models.

## 3.2 Materials and Methods

### 3.2.1 Experimental

Activated carbon (AC-A, AC-B, and AC-C) and carbon molecular sieve (CMS-A, CMS-B, CMS-C, and CMS-D) samples were provided by Xebec Adsorption Inc. (Blainville, QC, Canada) and are named sequentially rather than indicating adsorbent structure. The nitrogen (99.999%), oxygen (99.999%), and carbon dioxide (99.99%) gases used were purchased from Messer Inc. (Ottawa, ON, Canada).

Pure component gas adsorption isotherms were measured with a microgravimetric analyzer (VTI Corp., acquired by TA Instruments (New Castle, DE, USA)) at 16°C, 25°C, and 35°C. The adsorbents were regenerated at 150°C for 5 hours at a vacuum pressure of about $10^{-7}$ mbar. After regeneration, a helium adsorption isotherm was performed for use in buoyancy corrections. Afterwards, the adsorption isotherm experiment was performed up to 10 atm pressure. Desorption data points were then used to check for hysteresis.

### 3.2.2 Single-component adsorption isotherm models

To model the pure component adsorption isotherms, Langmuir and Sips models were used. The sum of square residuals was minimized to fit the model parameters.

In the Langmuir model (Eq. (3.1)), it is assumed that an adsorbent has a definite number of adsorption sites which are localized and that the energy of adsorption is constant for all sites. Each site is assumed to accommodate only one molecule in monolayer adsorption, with no interactions between adsorbate molecules. In practice, these assumptions may not necessarily be valid for a lot of adsorbent and adsorbate pairs, but the Langmuir model still fits the experimental data for a large number of systems.[9] The adsorption capacity $q$ is a function of the saturation monolayer adsorption capacity $q_m$, the Langmuir parameter $B$, and the pressure $P$.

$$q = \frac{q_m B P}{1 + BP} \tag{3.1}$$

The Sips model (Eq. (3.2)), also called the Langmuir-Freundlich model, has a similar form to the Langmuir isotherm, except there is an *n* term that represents the number of adsorption sites that a molecule occupies on the adsorbent.

$$q = \frac{q_m (BP)^{1/n}}{1 + (BP)^{1/n}} \tag{3.2}$$

The adsorbent's ideal selectivity for $CO_2$ over $N_2$ can be evaluated using the equilibrium adsorption capacity for the respective gases (Eq. (3.3)). This can be used as a performance parameter for the selection of the best adsorbent.

$$Ideal\ selectivity = \frac{q_{CO_2}}{q_{N_2}} \tag{3.3}$$

### 3.2.3 Isosteric heat of adsorption

The isosteric heat of adsorption values as a function of surface coverage were determined using the Clausius-Clapeyron equation (Eq. (3.4))[10,11] with data at temperature range between 16 and 35°C and pressures between 0 and 9.5 atm. The Sips adsorption model was used when calculating the heat of adsorption values. By plotting ln *P* as a function of 1/*T* at a constant surface loading of $q_e$, the isosteric heat of adsorption ($-\Delta H_{ads}$) can be found from the slope.

$$\frac{(-\Delta H_{ads})}{RT^2} = \left[\frac{\partial ln P}{\partial T}\right]_{q_e} \tag{3.4}$$

### 3.2.4 Predictive multicomponent adsorption models

To predict the binary isotherms, the Extended Langmuir Model (ELM) and the Ideal Adsorbed Solution Theory (IAST) were applied using the Langmuir model parameters from the pure component data. The Flory-Huggins Vacancy Solution Theory (FH-VST) was also used to predict the binary isotherms.

#### *3.2.4.1 Extended Langmuir Model (ELM)*

The ELM (Eq. (3.5)) makes the same assumptions as the pure component Langmuir model. The parameters from the pure component Langmuir model ($B$ and $q_i$) are used in the ELM to predict the binary adsorption isotherms. The Langmuir model was found to adequately represent the pure component isotherm data, so the ELM is an appropriate model to try to predict the multicomponent system behaviour. The fractional coverage of the adsorbent surface for component i, $\theta_i$, is the ratio of the amount adsorbed for component i, $q_i$, over its saturation adsorption capacity $q_{i,m}$.

$$\theta_i = \frac{q_i}{q_{i,m}} = \frac{B_i P_i}{1 + \sum_{j=1}^{n} B_j P_j} \tag{3.5}$$

#### *3.2.4.2 Ideal Adsorption Solution Theory (IAST)*

This model uses an analog of Raoult's law for adsorption, as shown in Eq. (3.6).

$$P y_{\mathrm{i}} = P_{\mathrm{i}}^{0} x_{\mathrm{i}} \tag{3.6}$$

$P$ is the total pressure, $y_i$ is the mole fraction of component i in the gas phase, $P^0_i$ is the equilibrium "vapor pressure" for pure i adsorption at the same spreading pressure, π, and the same temperature as the adsorbed mixture, and $x_i$ is the mole fraction of component i in the adsorbed phase. Ideal gas and ideal solution assumptions are made, i.e. the fugacity coefficients and the activity coefficients are equal to unity. It also assumes that the spreading pressure is the same for both components in the adsorbed phase at equilibrium, as shown in Eq. (3.7).[12]

$$\int_{0}^{P_1^0} \frac{q_1^0(P)}{P_1}\, dP = \frac{\pi_1 A}{RT} = \frac{\pi_2 A}{RT} = \int_{0}^{P_2^0} \frac{q_2^0(P)}{P_2}\, dP \tag{3.7}$$

$q^0_i$ is the adsorption capacity of pure component i as a function of $P$, $\pi_i$ is the spreading pressure for component i, $A$ is the surface area of adsorption, $R$ is the gas constant, and $T$ is the absolute temperature. Given there are no azeotropes in the system because of the ideal assumptions, IAST predictions using pure gas isotherm data collected for gases with small to moderate difference in polarity are likely to be accurate.[9] The total amount of gas adsorbed in the mixture, $q_t$, can be expressed by Eq. (3.8) by using $q^0_1$ and $q^0_2$ values determined at $P^0_1$ and $P^0_2$, respectively.

$$\frac{1}{q_t} = \frac{x_1}{q_1^0} + \frac{x_2}{q_2^0} \tag{3.8}$$

The pure component Langmuir model parameters were used for the IAST predictions since the Langmuir model represented the pure component data adequately.

#### *3.2.4.3 Flory Huggins-Vacancy Solution Theory (FH-VST)*

In the VST model,[13] the vacancy is accounted for as a separate component and the activity coefficients are predicted for each component in the mixture, including the vacancy. For example, the Flory Huggins model can be used for the prediction of the activity coefficients. Using the Flory Huggins model in conjunction with the VST model leads to the FH-VST model. The pure component VST isotherm for component i is derived from the Gibbs adsorption equation (Eq. (3.9)) and is written as the pressure $P$ as a function of the maximum adsorption capacity $q^\infty_i$, the Henry's law constant $b_i$, the fractional coverage $\theta$, and the parameter $\alpha_{iv}$.

$$P = \frac{q_i^\infty}{b_i}\left(\frac{\theta}{1-\theta}\right)\exp\left[\frac{\alpha_{iv}^2\theta}{1+\alpha_{iv}\theta}\right] \tag{3.9}$$

Where $\theta = \frac{q_i}{q_i^\infty}$ and $q_i$ is the amount adsorbed for component i at pressure $P$.

The activity coefficient for each component $\gamma^s_i$, including the vacancy, can be written as Eq. (3.10) using the Flory Huggins model.

$$ln\gamma_i^s = -\ln\left(\sum_{j=1}^{N}\frac{x_j^s}{\alpha_{ij}+1}\right) + \left[1 - \left(\sum_{j=1}^{N}\frac{x_j^s}{\alpha_{ij}+1}\right)^{-1}\right] \quad (3.10)$$

Where $\alpha_{ij} = \frac{\alpha_{iv}+1}{\alpha_{jv}+1} - 1$, $x_i^s = \frac{q_t x_i}{q_t^\infty}$, $x_v^s = 1 - \frac{q_t}{q_t^\infty}$, and $q_t^\infty = \sum_{i=1}^{N} x_i q_i^\infty$

Here, $x^s_i$ is the mole fraction of component i in a mixture including the vacancy in the adsorbed phase, and $q^\infty_t$ is the limiting amount adsorbed for the total mixture.

Finally, an expression for the gas and adsorbed phase equilibrium can be written for each component in the mixture as shown by Eq. (3.11). Here, $\varphi_i$ is the fugacity coefficient, which was assumed to be 1 for an ideal gas, and $\gamma^s_i$ are the activity coefficients. Using this system of equations, the binary mixture behaviour can be predicted. Because the model accounts for mixture non-ideality with the introduction of activity coefficients, this model is suitable for systems with azeotropes, as well.

$$y_i\varphi_i P = \gamma_i^s x_i \frac{q_t}{q_t^\infty}\frac{q_i^\infty}{b_i}\left[\frac{\exp\alpha_{iv}}{1+\alpha_{iv}}\right]\exp\left[\left(\frac{q_i^\infty - q_t^\infty}{q_t} - 1\right) ln(\gamma_v^s x_v^s)\right] \quad (3.11)$$

## 3.3 Results and Discussion

### 3.3.1 Adsorption Capacity

The experimental adsorption isotherm data were fit to the Langmuir and Sips adsorption isotherm models to find the best equation representing the adsorption behaviour. The Sips model was found to fit the data the best, but the Langmuir model also provided an adequate fit, such that Langmuir pure component parameters were used to predict the binary adsorption isotherms with the ELM and IAST models. The pure component adsorption isotherm VST model was also fit to the experimental pure component adsorption isotherm data for this model's parameters to be later used in prediction of binary mixture isotherms by FH-VST.

### *3.3.1.1 Carbon Molecular Sieves*

The experimental adsorption capacities of the adsorbents studied are shown in Figure 3.1 - Figure 3.4, together with corresponding Sips model fits. The parameters for the Langmuir, Sips, and VST model fits for the $CO_2$ and $N_2$ isotherm data are tabulated in Table 3.1 - Table 3.3. The Sips model was the best fit for the data, as shown by the low sum of square residual (SSR) values. For $CO_2$, the *n* values in the Sips model was about 1.4 for most of CMS, meaning a $CO_2$ molecule occupied about 1.4 adsorption sites on the adsorbent surface. Similarly, *n* values for $N_2$ were about 1.2, meaning an $N_2$ molecule occupied about 1.2 adsorption sites. The Langmuir and VST models provided a fairly good fit, especially at lower pressures.

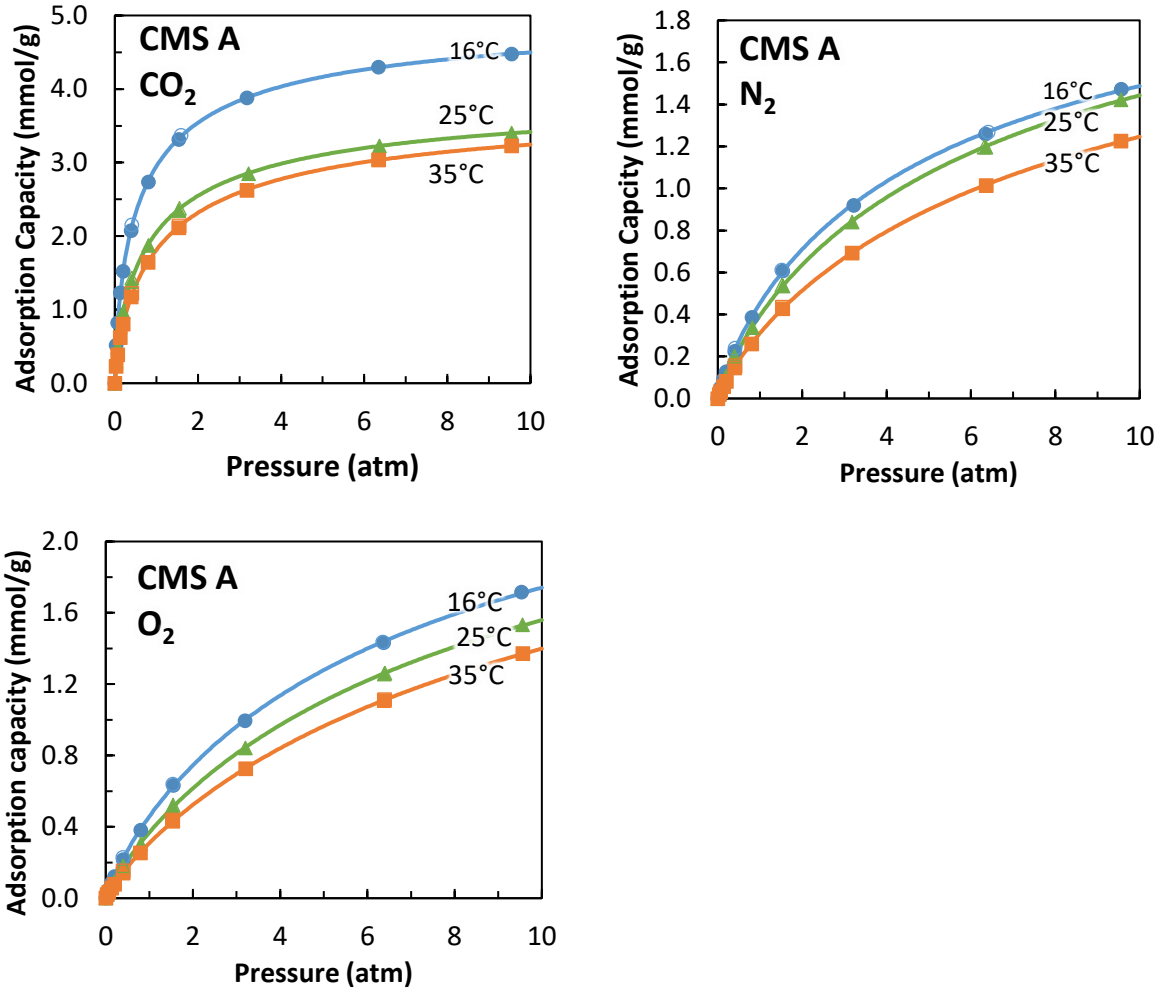


Figure 3.1 Adsorption isotherms of $CO_2$, $N_2$, and $O_2$ with CMS A at 16°C, 25°C, and 35°C. Curves represent Sips model fit.

For all the CMS samples, it was seen that the adsorption capacity decreased in the order of $CO_2$ >> $O_2$ ≥ $N_2$. These adsorbents showed clear selectivity for $CO_2$, while there was little difference between the adsorption capacities of $N_2$ and $O_2$. This general trend is consistent with the polarizability and the quadrupole moment of these gases, with $CO_2$ having the highest affinity to the adsorbent surface and the polarizability of $N_2$ and $O_2$ being similar.[14]

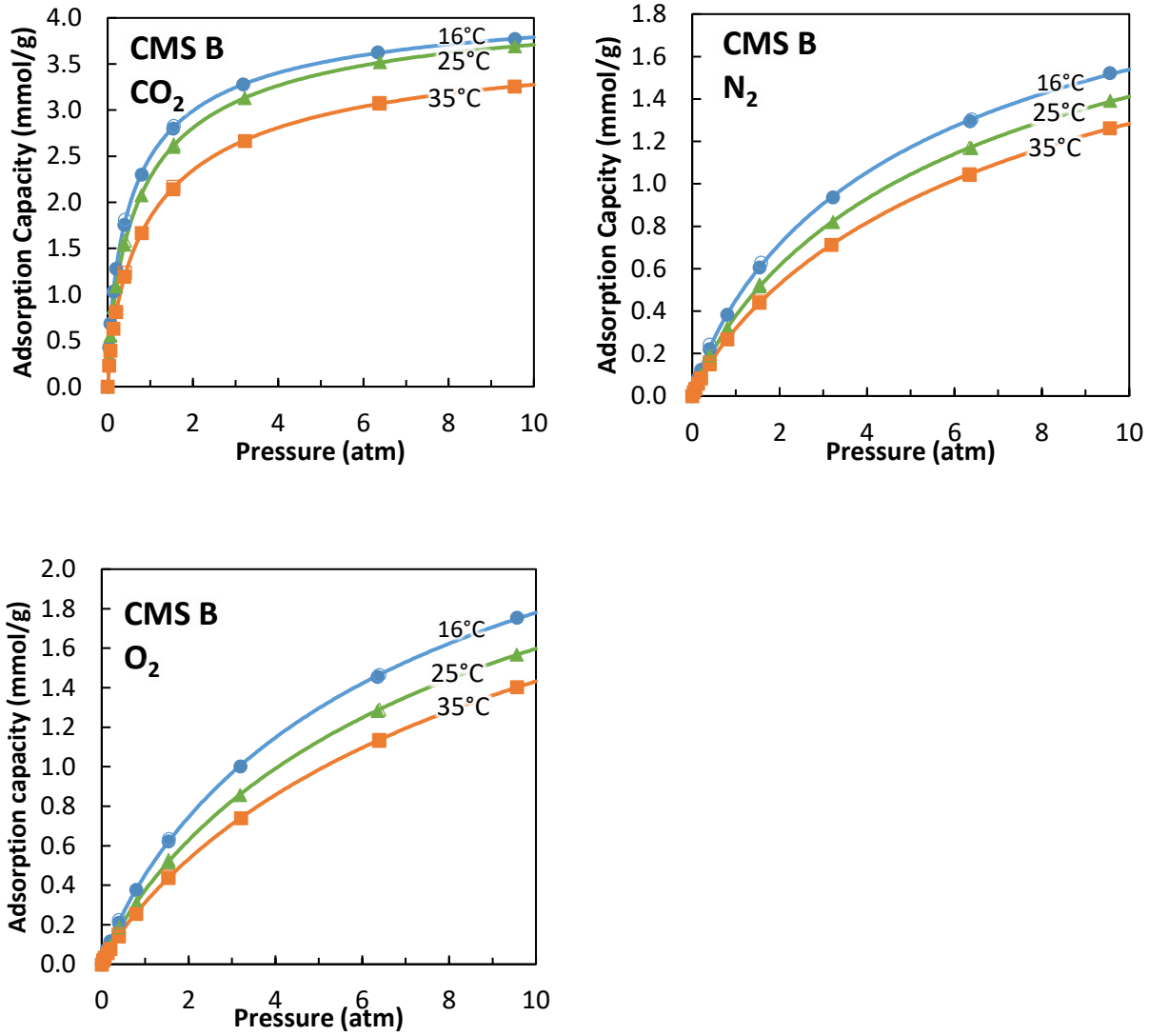


Figure 3.2 Adsorption isotherms of $CO_2$, $N_2$, and $O_2$ with CMS B at 16°C, 25°C, and 35°C. Curves represent Sips model fit.

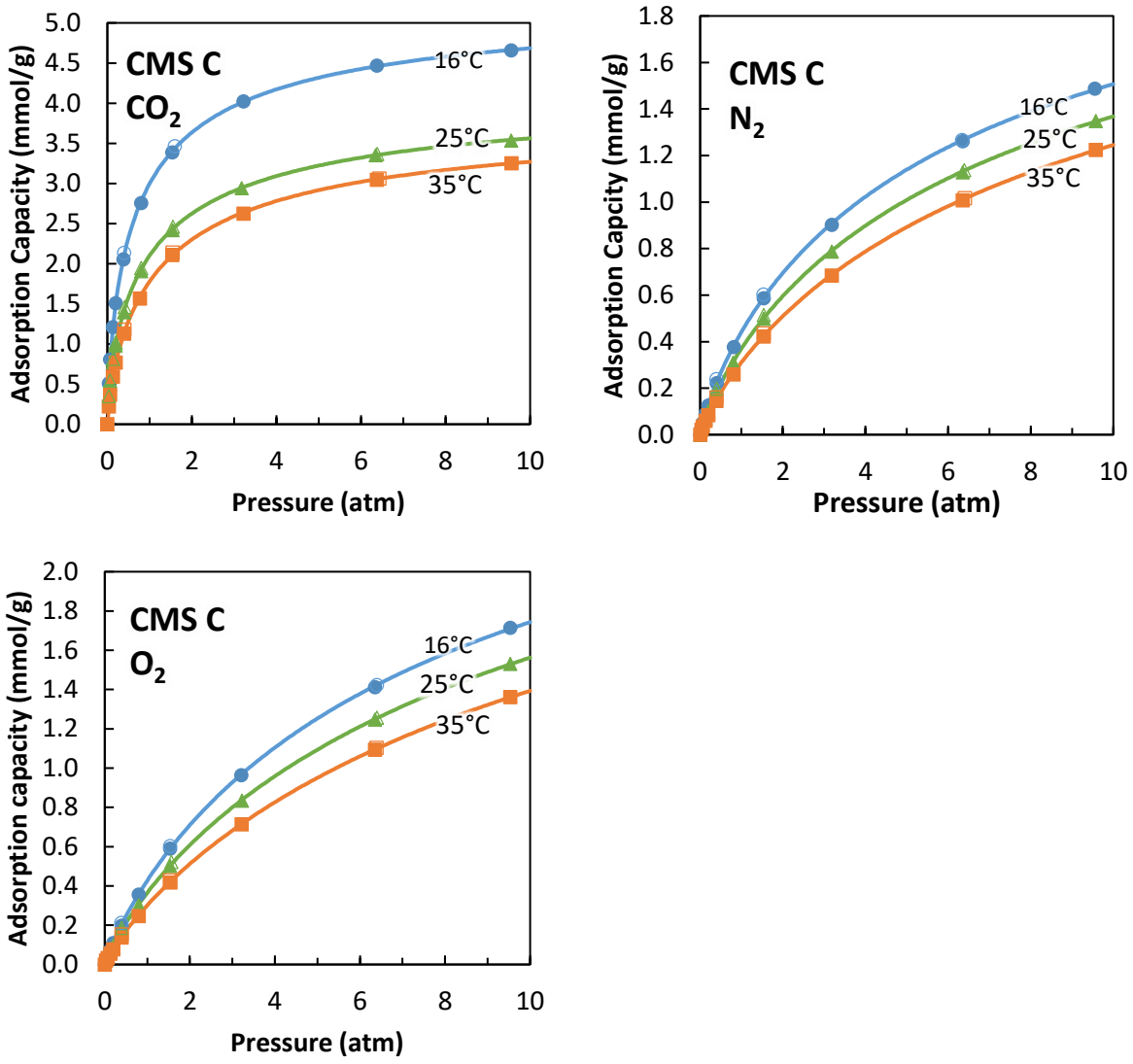


Figure 3.3 Adsorption isotherms of $CO_2$, $N_2$, and $O_2$ with CMS C at 16°C, 25°C, and 35°C. Curves represent Sips model fit.

It was observed that in all cases, the adsorption capacity decreased as temperature increased, as physical adsorption is an exothermic process. At 16°C, CMS-C had the highest $CO_2$ adsorption capacity. However, it was observed that CMS-B had the highest $CO_2$ adsorption capacity at 25°C, and CMS-D at 35°C. That said, the $CO_2$ adsorption capacity of all CMS samples tested were approximately equal at 35°C. The magnitude of the effect of temperature for different adsorbents varied. Since this effect is related to the isosteric heat of adsorption values, there is a discussion on those below.

For $N_2$ and $O_2$ gases, the adsorption capacities of all CMS samples at 16°C, 25°C, and 35°C were very similar within a given temperature, with the adsorption of $O_2$ being only slightly higher than that of $N_2$.

The desorption data points are shown in the isotherms as hollow points. It could be seen that the desorption points lined up very closely to the adsorption points, indicating there was not any hysteresis with any of the CMS samples.

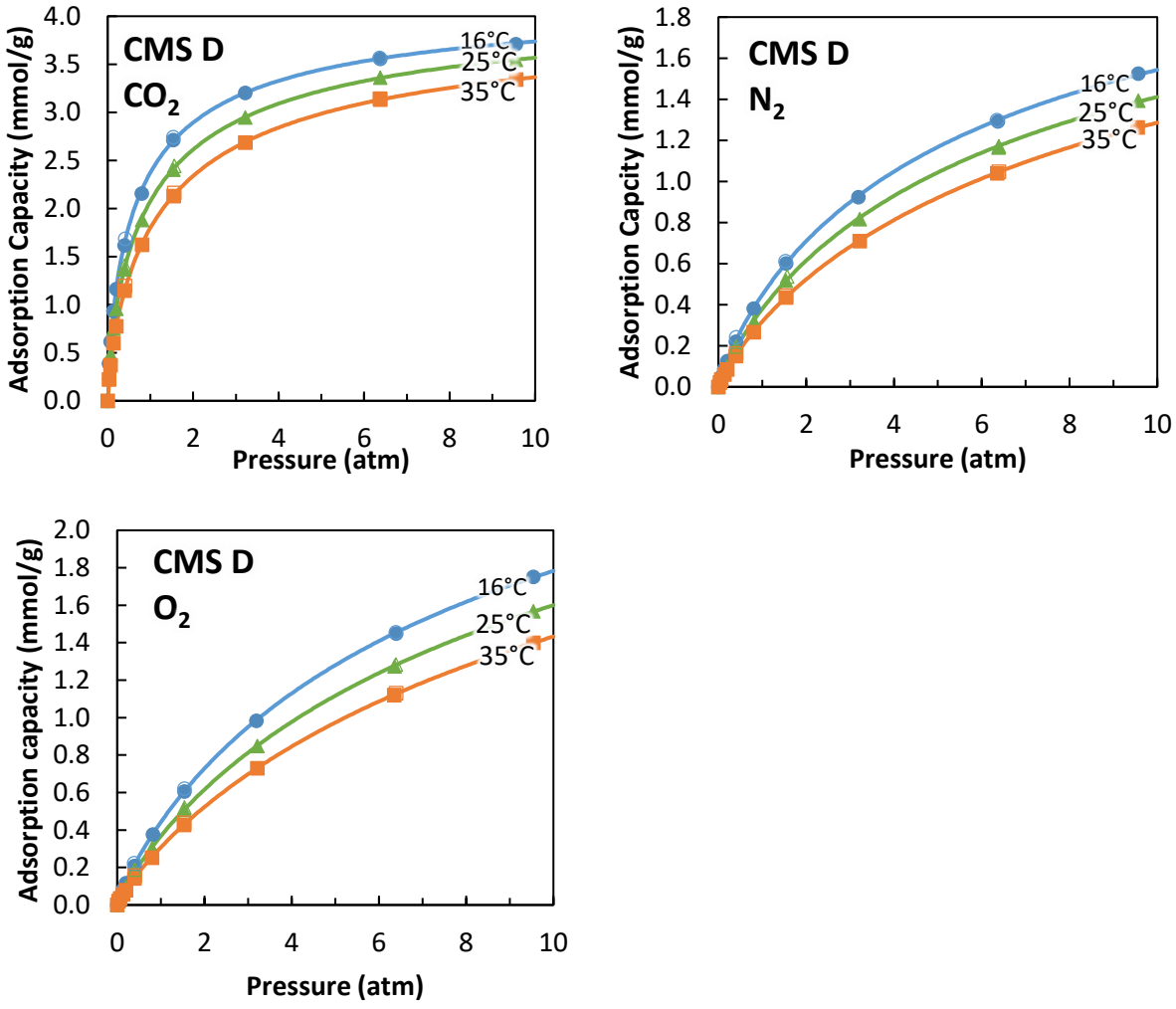


Figure 3.4 Adsorption isotherms of $CO_2$, $N_2$, and $O_2$ with CMS D at 16°C, 25°C, and 35°C. Curves represent Sips model fit.

Table 3.1 Langmuir, Sips, and VST model fit parameters for $CO_2$ isotherms with CMS samples at 16-35°C

| Adsorbent | Temperature | Langmuir | | | Sips | | | | VST | | | |
|---|---|---|---|---|---|---|---|---|---|---|---|---|
| | | $q_m$ | $B$ | $SSR$ | $q_m$ | $B$ | $n$ | $SSR$ | $n_1^\infty$ | $b_1$ | $\alpha_{1v}$ | $SSR$ |
| | °C | mol kg$^{-1}$ | atm$^{-1}$ | mol kg$^{-1}$ | mol kg$^{-1}$ | atm$^{-1}$ | - | mol kg$^{-1}$ | mol kg$^{-1}$ | mol kg$^{-1}$ atm$^{-1}$ | - | mol kg$^{-1}$ |
| CMS-A | 16 | 4.467 | 2.305 | 0.277 | 5.126 | 1.519 | 1.382 | 2.25E-03 | | | | |
| | 25 | 3.459 | 1.663 | 0.142 | 4.021 | 1.052 | 1.359 | 1.63E-03 | 3.7935 | 6.1187 | 1.1350 | 0.099 |
| | 35 | 3.348 | 1.310 | 0.109 | 3.908 | 0.824 | 1.329 | 1.56E-03 | | | | |
| CMS-B | 16 | 3.774 | 2.291 | 0.183 | 4.298 | 1.549 | 1.364 | 1.33E-03 | | | | |
| | 25 | 3.750 | 1.762 | 0.155 | 4.305 | 1.162 | 1.341 | 1.46E-03 | 4.0177 | 4.8781 | 0.1840 | 0.290 |
| | 35 | 3.402 | 1.301 | 0.153 | 3.924 | 0.846 | 1.317 | 2.07E-03 | | | | |
| CMS-C | 16 | 4.676 | 2.106 | 0.291 | 5.382 | 1.370 | 1.375 | 3.97E-03 | | | | |
| | 25 | 3.585 | 1.680 | 0.273 | 4.256 | 0.967 | 1.386 | 5.60E-03 | 3.9343 | 4.2833 | 0.5165 | 0.159 |
| | 35 | 3.435 | 1.165 | 0.095 | 3.955 | 0.770 | 1.305 | 2.13E-03 | | | | |
| CMS-D | 16 | 3.787 | 1.939 | 0.163 | 4.270 | 1.350 | 1.335 | 4.88E-03 | | | | |
| | 25 | 3.642 | 1.500 | 0.145 | 4.240 | 0.948 | 1.346 | 1.87E-03 | 3.9428 | 4.3516 | 0.5148 | 0.165 |
| | 35 | 3.543 | 1.115 | 0.106 | 4.125 | 0.714 | 1.319 | 9.18E-04 | | | | |

Table 3.2 Langmuir, Sips, and VST model fit parameters for $N_2$ isotherms with CMS samples at 16-35°C

| Adsorbent | Temperature | Langmuir | | | Sips | | | | VST | | | |
|---|---|---|---|---|---|---|---|---|---|---|---|---|
| | | $q_m$ | $B$ | $SSR$ | $q_m$ | $B$ | $n$ | $SSR$ | $n_1^\infty$ | $b_1$ | $\alpha_{1v}$ | $SSR$ |
| | °C | mol kg$^{-1}$ | atm$^{-1}$ | mol kg$^{-1}$ | mol kg$^{-1}$ | atm$^{-1}$ | - | mol kg$^{-1}$ | mol kg$^{-1}$ | mol kg$^{-1}$ atm$^{-1}$ | - | mol kg$^{-1}$ |
| CMS-A | 16 | 1.9442 | 0.2992 | 4.84E-03 | 2.3598 | 0.1866 | 1.1693 | 5.05E-04 | | | | |
| | 25 | 2.0076 | 0.2388 | 3.67E-03 | 2.4964 | 0.1441 | 1.1599 | 2.64E-04 | 2.5617 | 0.5857 | 1.3216 | 5.06E-03 |
| | 35 | 1.8545 | 0.1959 | 1.99E-03 | 2.3149 | 0.1191 | 1.1430 | 1.53E-04 | | | | |
| CMS-B | 16 | 2.0567 | 0.2759 | 4.74E-03 | 2.4847 | 0.1756 | 1.1569 | 7.31E-04 | | | | |
| | 25 | 1.9917 | 0.2287 | 2.98E-03 | 2.4394 | 0.1436 | 1.1455 | 2.58E-04 | 2.1847 | 0.4203 | 0.2981 | 9.48E-02 |
| | 35 | 1.9120 | 0.1940 | 2.10E-03 | 2.3863 | 0.1189 | 1.1394 | 1.44E-04 | | | | |
| CMS-C | 16 | 2.0070 | 0.2753 | 6.13E-03 | 2.5499 | 0.1550 | 1.1922 | 6.96E-04 | | | | |
| | 25 | 1.9163 | 0.2323 | 4.13E-03 | 2.4627 | 0.1301 | 1.1773 | 4.89E-04 | 2.5537 | 0.5509 | 1.4267 | 1.45E-02 |
| | 35 | 1.8455 | 0.1950 | 2.92E-03 | 2.4411 | 0.1049 | 1.1714 | 2.73E-04 | | | | |
| CMS-D | 16 | 2.0693 | 0.2704 | 5.41E-03 | 2.5744 | 0.1606 | 1.1752 | 6.04E-04 | | | | |
| | 25 | 1.9855 | 0.2303 | 3.59E-03 | 2.4670 | 0.1398 | 1.1553 | 5.62E-04 | 2.6821 | 0.5875 | 1.5067 | 8.97E-03 |
| | 35 | 1.9180 | 0.1919 | 2.77E-03 | 2.5049 | 0.1064 | 1.1624 | 2.11E-04 | | | | |

The isosteric heat of adsorption values ($-\Delta H_{ads}$) for $CO_2$ and $N_2$ are shown in Figure 3.5 for CMS A-D samples. As expected, the values for the heat of adsorption for $CO_2$ were larger than those for $N_2$ and $O_2$ due its higher polarizability and quadrupole moment. CMS-A and CMS-C had the highest isosteric heat for $CO_2$. The isosteric heat of CMS-B for $CO_2$ was much lower than them, and CMS-D had the lowest isosteric heat of adsorption for $CO_2$.

Table 3.3 Langmuir, Sips, and VST model fit parameters for $O_2$ isotherms with CMS samples at 16-35°C

| Adsorbent | Temperature | Langmuir | | | Sips | | | |
|---|---|---|---|---|---|---|---|---|
| | | $q_m$ | $B$ | $SSR$ | $q_m$ | $B$ | $n$ | $SSR$ |
| | °C | mmol $g^{-1}$ | $atm^{-1}$ | mmol $g^{-1}$ | mmol $g^{-1}$ | $atm^{-1}$ | - | mmol $g^{-1}$ |
| CMS-A | 16 | 2.4895 | 0.2192 | 4.80E-03 | 3.0911 | 0.1340 | 1.1490 | 6.03E-04 |
| | 25 | 2.4149 | 0.1742 | 2.80E-03 | 3.0346 | 0.1065 | 1.1319 | 3.00E-04 |
| | 35 | 2.2964 | 0.1495 | 2.29E-03 | 3.0201 | 0.0846 | 1.1375 | 2.23E-04 |
| CMS-B | 16 | 2.6097 | 0.2038 | 3.94E-03 | 3.1925 | 0.1299 | 1.1329 | 4.28E-04 |
| | 25 | 2.4896 | 0.1712 | 2.89E-03 | 3.1485 | 0.1034 | 1.1334 | 2.20E-04 |
| | 35 | 2.3733 | 0.1462 | 2.22E-03 | 3.0969 | 0.0843 | 1.1318 | 2.26E-04 |
| CMS-C | 16 | 2.6214 | 0.1890 | 3.83E-03 | 3.2534 | 0.1176 | 1.1331 | 5.40E-04 |
| | 25 | 2.4382 | 0.1691 | 4.04E-03 | 3.2974 | 0.0885 | 1.1640 | 3.59E-04 |
| | 35 | 2.3306 | 0.1423 | 2.58E-03 | 3.1717 | 0.0756 | 1.1462 | 3.22E-04 |
| CMS-D | 16 | 2.6553 | 0.1932 | 4.98E-03 | 3.4127 | 0.1109 | 1.1547 | 4.73E-04 |
| | 25 | 2.5347 | 0.1631 | 3.57E-03 | 3.3541 | 0.0900 | 1.1494 | 3.35E-04 |
| | 35 | 2.4096 | 0.1403 | 2.78E-03 | 3.3371 | 0.0721 | 1.1513 | 2.61E-04 |

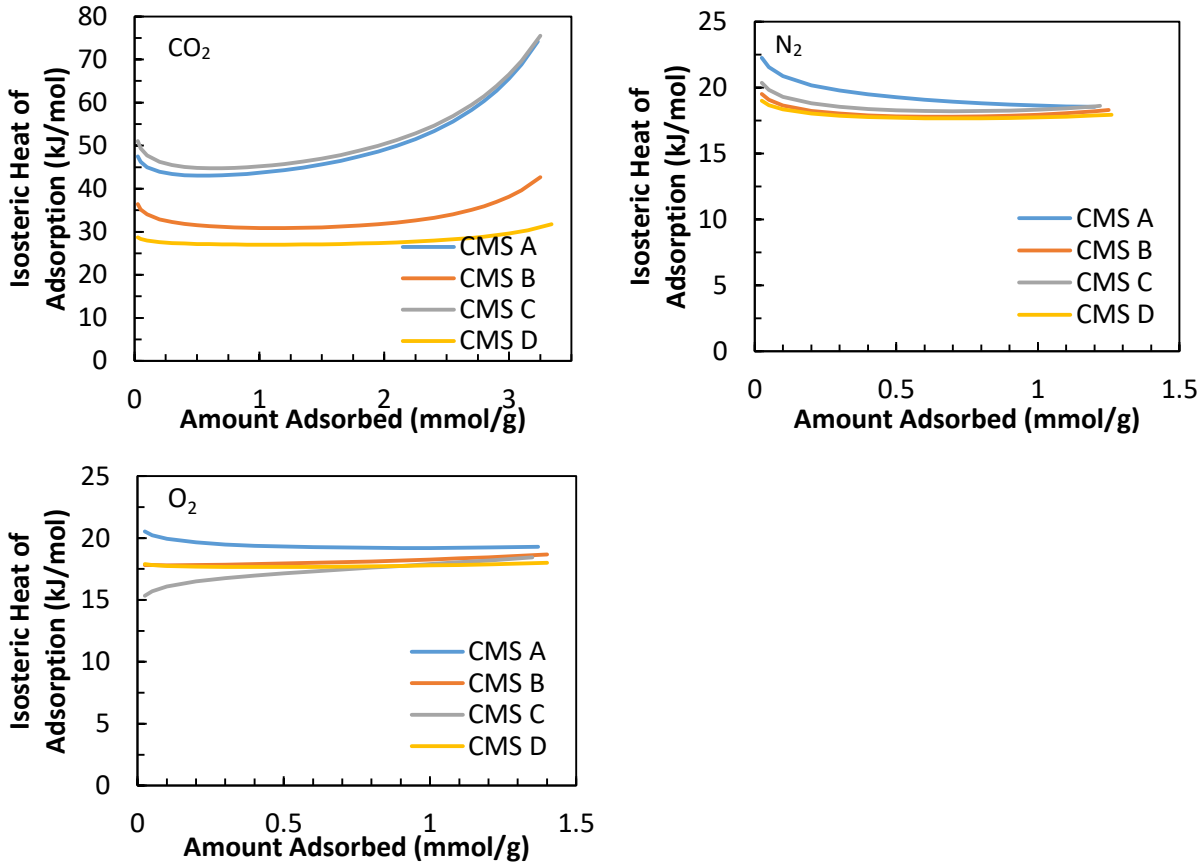


Figure 3.5 Isosteric heat of adsorption values of CMS A-D samples for $CO_2$, $N_2$ and $O_2$ gases.

These trends in the isosteric heat of adsorption values match the behaviour observed in the $CO_2$ adsorption isotherms as *T* increases, especially for CMS-A and CMS-C where the $CO_2$ adsorption capacity was much higher at 16°C than at 25°C. The magnitude of the isosteric heat of adsorption for $CO_2$ is quite high compared to other adsorbents in the literature.[8,15–17] However, the values for $N_2$ and $O_2$ are similar to other carbon based adsorbents.

The CMS samples showed good $CO_2/N_2$ selectivity, with trends in the selectivity with respect to pressure varying depending on the temperature, as illustrated in Figure 3.6. In general, as the temperature increased, the $CO_2/N_2$ selectivity decreased. At 16°C and 35°C, CMS-C showed the highest $CO_2/N_2$ selectivity, though at 35°C, the selectivity values of all CMS samples were very similar. However, at 25°C, CMS-B was the CMS that showed the highest $CO_2/N_2$ selectivity.

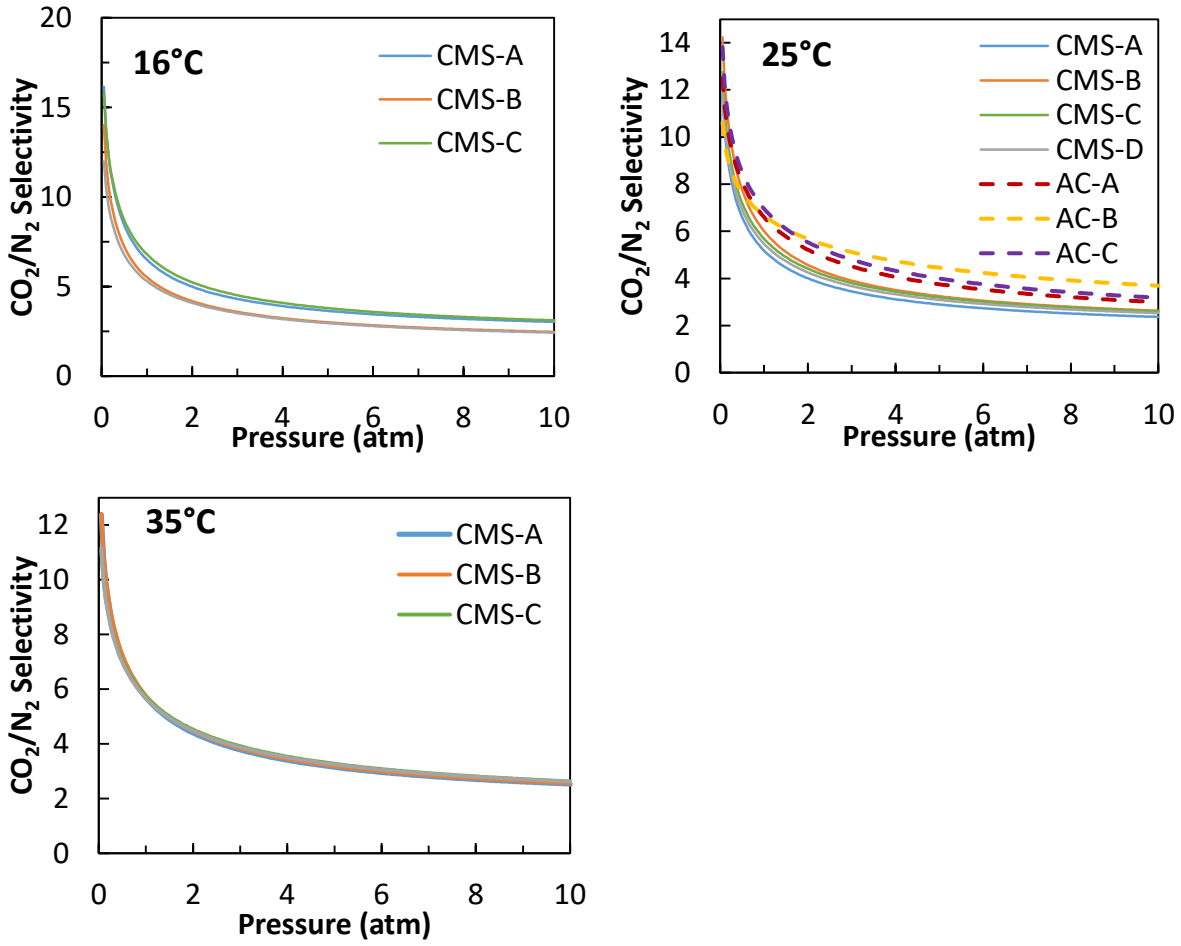


Figure 3.6 $CO_2/N_2$ equilibrium selectivity values with CMS samples at 16°C, 25°C, and 35°C and with AC samples at 25°C.

The selectivity decreased greatly as pressure increased, which is expected and can be explained by the shape of the $CO_2$ and $N_2$ isotherms in Figure 3.1 - Figure 3.4, where the $CO_2$ isotherms have a more rectangular shape, while the $N_2$ isotherms have a more linear trend as pressure increases.

### *3.3.1.2 Activated Carbons*

The $CO_2$ and $N_2$ adsorption isotherms for the activated carbon samples at 25°C are shown in Figure 3.7, with Langmuir, Sips, and VST model parameters tabulated in Table 3.4. Similar to CMS samples, the Sips model was the best fit, with Langmuir and VST providing decent fits. At low to moderate pressure (<1.5 atm), the $CO_2$ adsorption capacity of AC-C was slightly higher than that of AC-B. However, at higher pressures, the $CO_2$ adsorption capacity of AC-B was significantly higher than that of AC-C. Because the adsorption capacity of AC-C at low pressures was only marginally larger than that of AC-B, it could be said that overall, AC-B had the highest $CO_2$ adsorption capacity of the activated carbons tested. AC-A had the lowest $CO_2$ and $N_2$ adsorption capacities. It was also observed that no hysteresis occurred, as the desorption points coincided well with the adsorption points for all the AC samples.

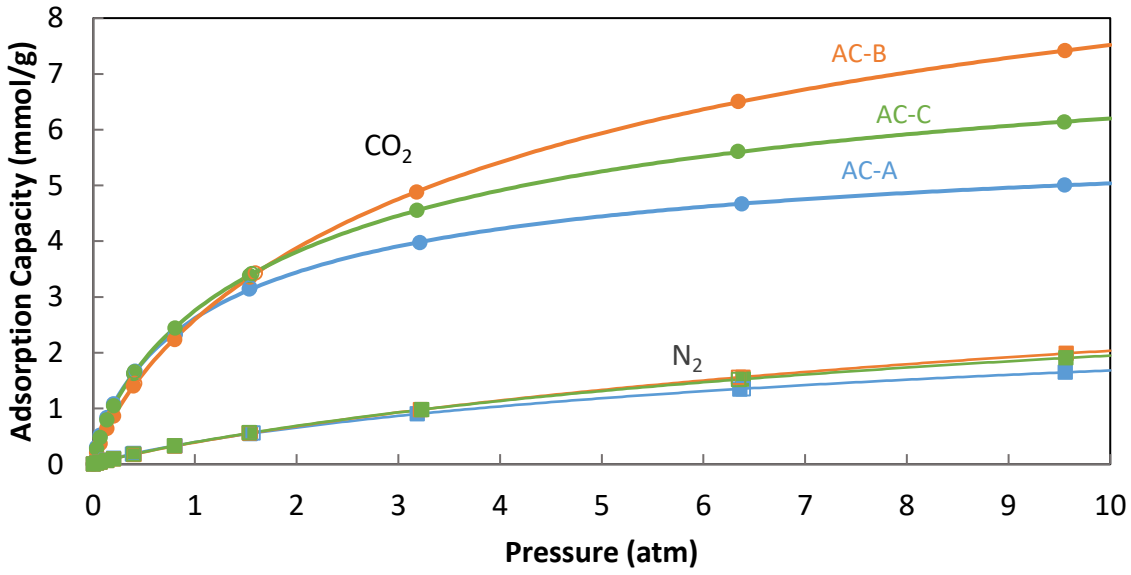


Figure 3.7 $CO_2$ and $N_2$ adsorption isotherms with AC samples at 25°C. Curves represent Sips model fit.

In Figure 3.6, the $CO_2/N_2$ selectivity values for the activated carbon samples at 25°C are also shown. The adsorbent with the highest $CO_2/N_2$ selectivity at 25°C was AC-C below about 1.5 atm, and was AC-B above 1.5 atm. AC-A had the lowest $CO_2/N_2$ selectivity values. This is the same trend as the $CO_2$ adsorption capacities.

Table 3.4 Langmuir, Sips, and VST model fit parameters for $CO_2$ and $N_2$ isotherms with AC samples at 25°C

| Adsorbent | Adsorbate | Langmuir | | | Sips | | | | VST | | | |
|---|---|---|---|---|---|---|---|---|---|---|---|---|
| | | $q_m$ | $B$ | $SSR$ | $q_m$ | $B$ | $n$ | $SSR$ | $n_1^\infty$ | $b_1$ | $\alpha_{1v}$ | $SSR$ |
| | | mol kg$^{-1}$ | atm$^{-1}$ | mol kg$^{-1}$ | mol kg$^{-1}$ | atm$^{-1}$ | - | mol kg$^{-1}$ | mol kg$^{-1}$ | mmol kg$^{-1}$ atm$^{-1}$ | - | mol kg$^{-1}$ |
| AC-A | $CO_2$ | 5.3233 | 1.0420 | 2.07E-01 | 6.2000 | 0.6662 | 1.2942 | 3.66E-03 | 5.9401 | 13.4333 | 2.1634 | 1.03E-02 |
| | $N_2$ | 2.6094 | 0.1722 | 4.07E-03 | 3.4655 | 0.0935 | 1.1584 | 7.40E-05 | 3.6219 | 0.5333 | 1.3594 | 2.71E-03 |
| AC-B | $CO_2$ | 9.1987 | 0.3894 | 2.57E-01 | 11.7818 | 0.2041 | 1.2569 | 1.10E-03 | 11.0130 | 5.0330 | 1.4957 | 2.36E-03 |
| | $N_2$ | 3.8967 | 0.1065 | 2.75E-03 | 5.1977 | 0.0614 | 1.1102 | 7.28E-05 | 4.7916 | 0.4244 | 0.7576 | 1.77E-02 |
| AC-C | $CO_2$ | 6.8432 | 0.7011 | 2.87E-01 | 8.3404 | 0.3988 | 1.3005 | 8.93E-04 | 7.7500 | 7.8837 | 1.6557 | 8.41E-04 |
| | $N_2$ | 3.4729 | 0.1243 | 2.20E-03 | 4.3349 | 0.0800 | 1.0991 | 9.62E-05 | 5.0178 | 0.4847 | 1.2604 | 3.38E-04 |

Comparing the activated carbon and CMS samples, it was clear that activated carbons had higher adsorption capacities than CMS samples at 25°C. This was expected, as activated carbons have higher surface area and a wider pore size distribution.[6] Furthermore, as seen in Figure 3.6, activated carbon samples had higher $CO_2/N_2$ selectivity values than the CMS samples at the same temperature. For applications where the partial pressure of $CO_2$ will be low, like combustion flue gas applications, AC-C would be appropriate, as it had high $CO_2/N_2$ selectivity and $CO_2$ adsorption capacity compared to the other samples at 25°C.

### 3.3.2 Comparison to Adsorbents in the Literature

The pure component $CO_2$ and $N_2$ adsorption capacities of various commercial adsorbents found in literature are presented in Table 3.5 at 20-40°C and 1 atm and compared to the results obtained in this work. LiX had the highest $q_{CO_2}$ in Table 3.5, and 2GA-H2J AC had the second highest $q_{CO_2}$. The AC and CMS samples in this study were found to have comparable $CO_2$ adsorption capacities as other AC and CMS in the literature under similar conditions, and slightly higher $N_2$ adsorption capacities. AC-B, which had the highest $CO_2$ adsorption capacity from this study, had a 17.6% higher $q_{CO_2}$ than the average of other studies in Table 3.5. AC-B had a similar

$q_{CO_2}$ as 2GA-H2J AC but a higher ideal $CO_2/N_2$ selectivity, which is quite good. The adsorbent with the highest $CO_2/N_2$ ideal selectivity in Table 3.5 was Norit AC, which was higher than the average $CO_2/N_2$ ideal selectivity of the AC and CMS samples in this study. However, the $CO_2/N_2$ ideal selectivities of the AC and CMS samples from this study were overall similar to those in the literature other than Norit AC and 13X.

Table 3.5 $CO_2$ and $N_2$ adsorption of commercially available adsorbents at 1 atm and 20-40°C

| Source | Adsorbent | $T$ °C | $q_{CO_2}$ mmol $g^{-1}$ | $q_{N_2}$ mmol $g^{-1}$ | $CO_2/N_2$ Ideal Selectivity | Reference |
|---|---|---|---|---|---|---|
| Zeochem Co. | LiX | 20 | 4.635 | 0.775 | 5.98 | [15] |
| Kuraray Chemical Co. | 2GA-H2J AC | 20 | 2.762 | 0.439 | 6.29 | [15] |
| Activated Carbon NZ Ltd. | NZ-AC | 30 | 2.527 | 0.317 | 7.97 | [16] |
| Norit Activated Carbon | Norit AC | 40 | 2.130 | 0.200 | 10.65 | [18] |
| Calgon Carbon | BPL AC | 25 | 2.081 | 0.285 | 7.31 | [19] |
| Kuraray Chemical Co. | CMS | 25 | 2.028 | 0.357 | 5.68 | [8] |
| Sigma Aldrich | 13X | 25 | 1.716 | 0.165 | 10.41 | [19] |
| Air Products and Chemicals Inc. | CMS A | 30 | 1.630 | 0.295 | 5.53 | [20] |
| Takeda Chemical Company | CMS-T3A | 30 | 1.559 | 0.256 | 6.08 | [21] |
| Xebec Adsorption Inc. | AC-A | 25 | 2.594 | 0.397 | 6.54 | This work |
| Xebec Adsorption Inc. | AC-B | 25 | 2.755 | 0.389 | 7.08 | This work |
| Xebec Adsorption Inc. | AC-C | 25 | 2.129 | 0.396 | 5.38 | This work |
| Xebec Adsorption Inc. | CMS-A | 25 | 2.048 | 0.395 | 5.18 | This work |
| Xebec Adsorption Inc. | CMS-B | 25 | 2.273 | 0.379 | 6.00 | This work |
| Xebec Adsorption Inc. | CMS-C | 25 | 2.102 | 0.370 | 5.68 | This work |
| Xebec Adsorption Inc. | CMS-D | 25 | 2.077 | 0.380 | 5.47 | This work |

### 3.3.3 Prediction of Mixture Adsorption Behaviour

The $CO_2$-$N_2$ binary gas mixture adsorption isotherms were all predicted at 25°C for 1 atm total pressure using the ELM, IAST, and FH-VST models for both the CMS and activated carbon samples. While these predictions may not necessarily be the same as experimental binary mixture adsorption isotherms, they provide insight into the possible performance of these adsorbents in a mixture.

Figure 3.8 shows the predicted $CO_2$-$N_2$ binary adsorption isotherms with all the CMS samples. The models predicted similar behaviour for these adsorbents, however FH-VST predicted a smaller $CO_2$ and slightly higher $N_2$ adsorption capacity for the CMS samples.

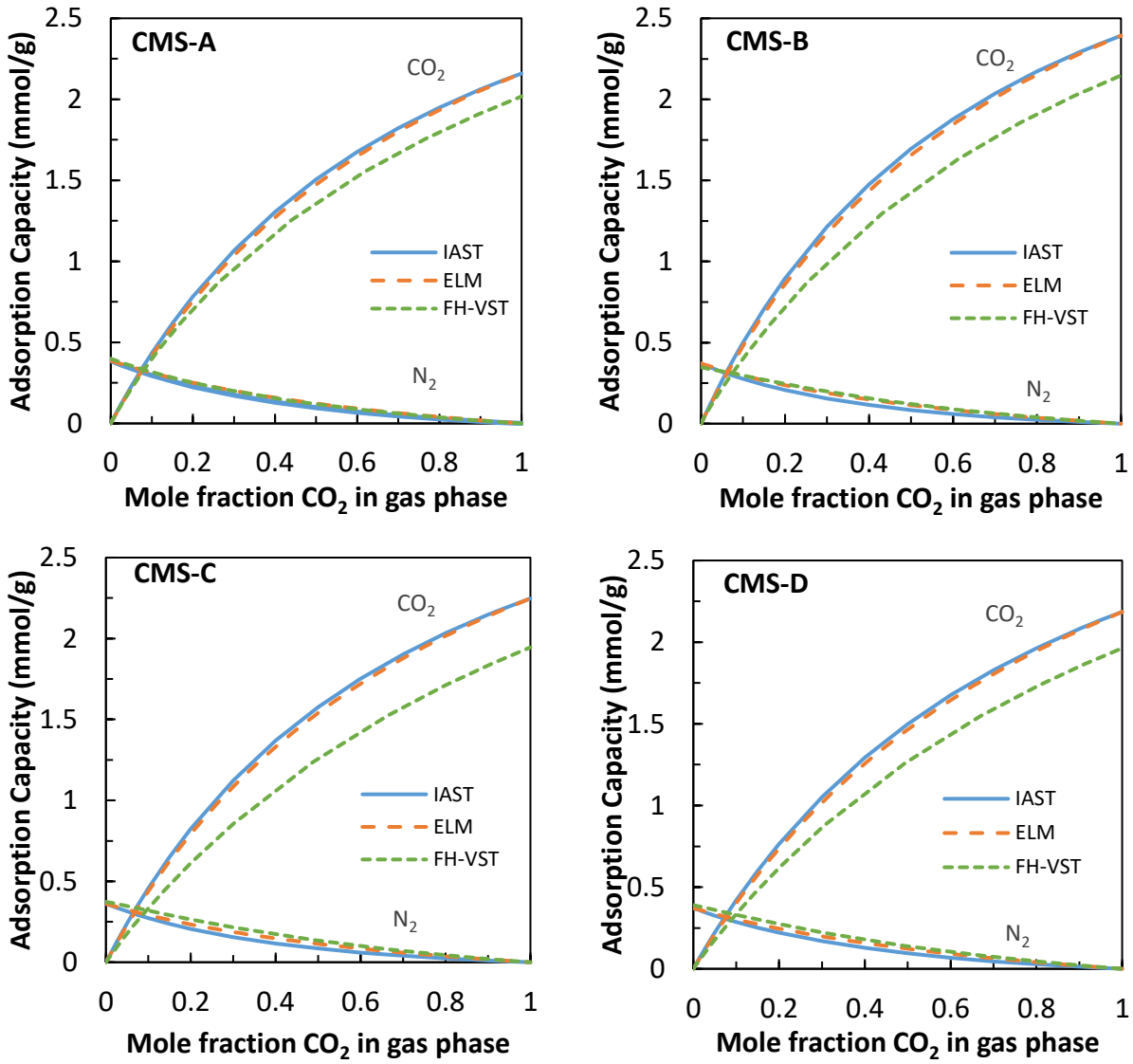


Figure 3.8 Predicted $CO_2$-$N_2$ binary adsorption isotherms with CMS samples at 25°C and 1 atm. total pressure.

FH-VST predicted a slightly worse separation between the $CO_2$ and $N_2$, as can be seen in the X-Y diagrams in Figure 3.9, where the FH-VST predictions are closer to the 45° line than the ELM or IAST predictions. However, the curves are still far away from the 45° line, showing that separation is easy between the two gases, no matter which adsorbent is used. As it was seen with

the pure component isotherms for CMS, the adsorbent with the best $CO_2/N_2$ separation was CMS-B no matter which binary prediction model was considered.

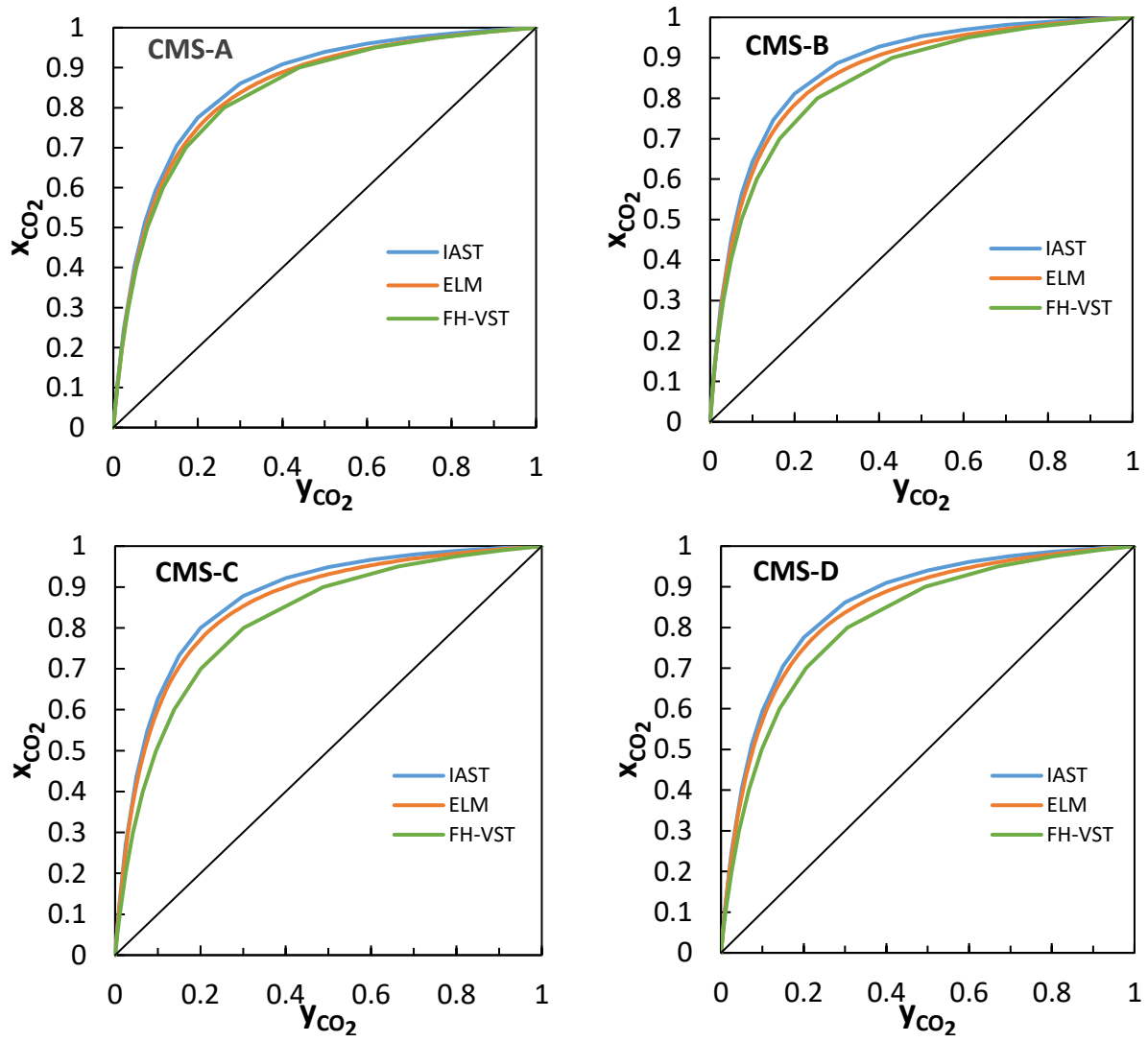


Figure 3.9 Predicted phase diagrams for $CO_2$-$N_2$ binary mixture with CMS samples at 25°C and 1 atm. total pressure.

The predicted $CO_2$-$N_2$ binary adsorption isotherms at 25°C and 1 atm total pressure for the activated carbon samples are shown in Figure 3.10. For the AC samples, FH-VST predicted higher adsorption capacities than ELM or IAST, with ELM and IAST showing very similar capacities. At $y_{CO_2} = 1$, for AC samples, the adsorption capacity of $CO_2$ predicted by ELM and IAST was closer to the corresponding pure component isotherm data at 1 atm pressure, while FH-VST slightly overestimated it. For this reason, IAST and ELM likely predict the $CO_2$-$N_2$ binary

adsorption with these activated carbons more accurately than FH-VST. As observed with the pure component isotherms, the adsorption capacity of $CO_2$ was the lowest with AC-B at 1 atm. In the three prediction models used, the adsorption capacities of $CO_2$ with AC-A and with AC-C were similar, with AC-A being slightly higher than AC-C until $y_{CO_2} = 0.65$, after which AC-C had the greater $CO_2$ adsorption. $N_2$ adsorption capacities were similar for all activated carbons tested, with AC-B having slightly higher amounts adsorbed.

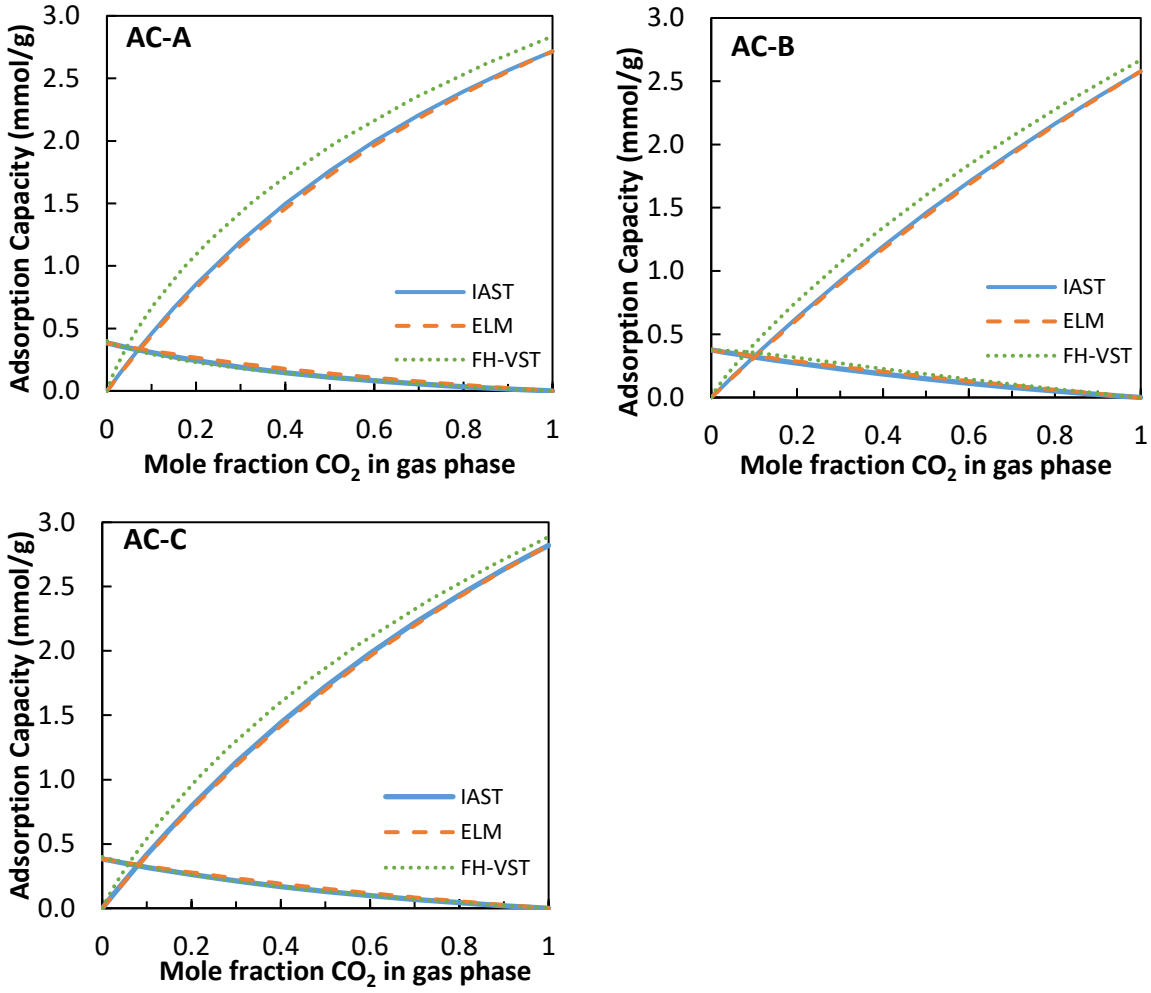


Figure 3.10 Predicted $CO_2$-$N_2$ binary adsorption isotherms for AC samples at 25°C and 1 atm. total pressure.

The corresponding phase diagram predictions for the activated carbons at 25°C and 1 atm total pressure in Figure 3.11 show that AC-A had the highest $CO_2/N_2$ selectivity (with its plot being

the furthest away from the 45 degree line), followed by AC-C, then AC-B. This is a similar trend to the adsorption capacity of $CO_2$ in the binary mixture.

Comparing the predictions for activated carbons with CMS's, again the activated carbons had higher $CO_2$ adsorption capacities. However, the difference between the two was not large at 25°C and 1 atm.

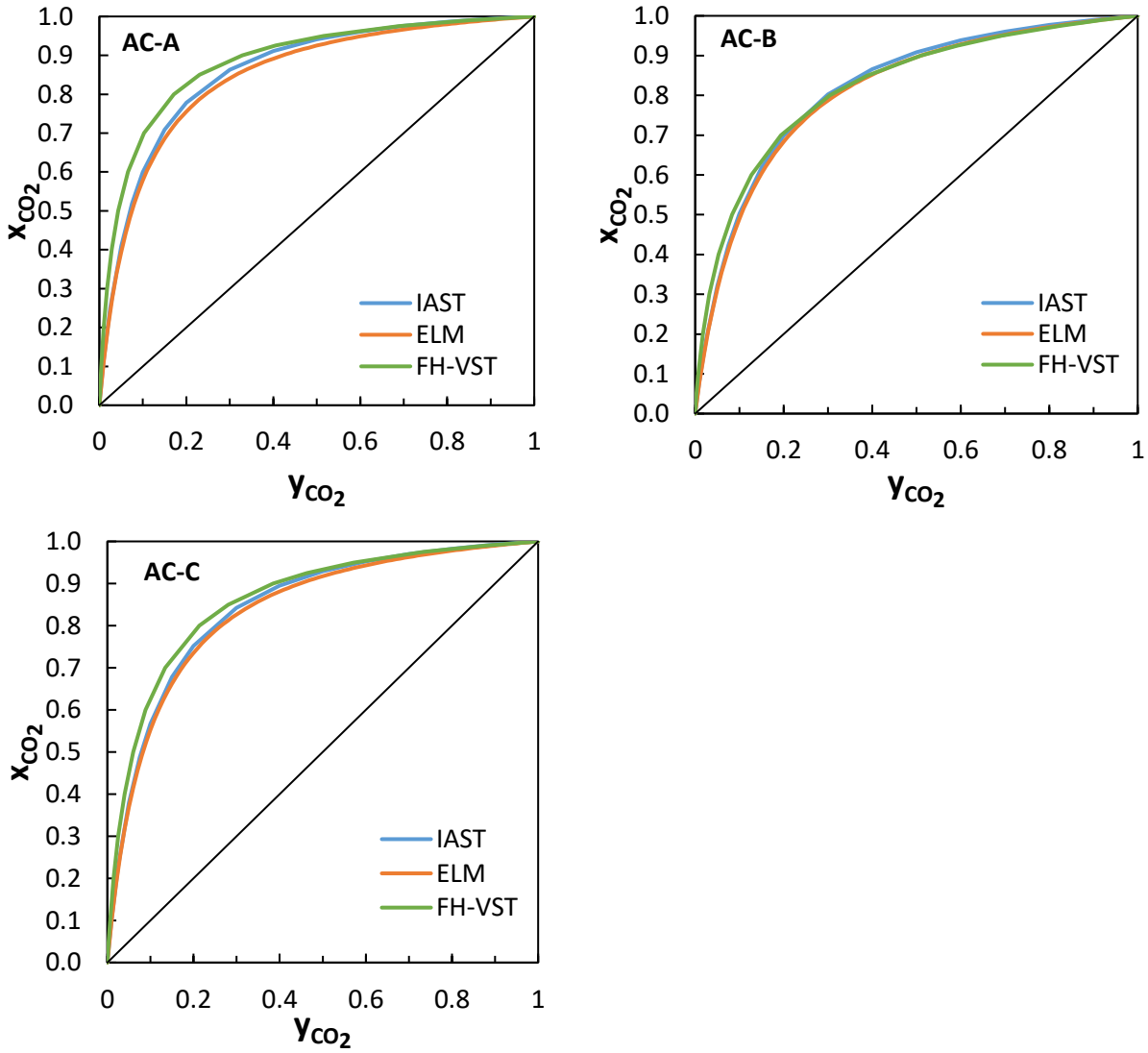


Figure 3.11 Predicted phase diagrams for $CO_2$-$N_2$ binary mixture with AC samples at 25°C and 1 atm. total pressure.

## 3.4 Conclusions

In this study, pure component adsorption capacities of $CO_2$ and $N_2$ were measured on commercially available AC and CMS adsorbents at 25°C. Isotherm data were also obtained at 16°C and 35°C for CMS samples, as well as $O_2$ adsorption isotherms. Of the samples tested, AC-B exhibited the highest $CO_2$ adsorption capacity above 1.5 atm. Also, as expected, the adsorption capacities decreased as temperature increased. $CO_2/N_2$ selectivity values also decreased as temperature increased. At 25°C, the adsorbent that had the highest $CO_2/N_2$ selectivity was AC-C below 1.5 atm, and was AC-B above 1.5 atm. At 16°C and 35°C, CMS-C had the highest $CO_2/N_2$ selectivity. The isosteric heat of adsorption values for $CO_2$, $N_2$, and $O_2$ were calculated for the CMS samples and they were comparable to other carbon adsorbents in the literature, except for CMS-A and CMS-C having higher value for $CO_2$, at more than 40 kJ/mol.

The AC and CMS samples in this study had similar adsorption capacities and $CO_2/N_2$ selectivities as other commercially available adsorbents reported in the literature, though AC-B showed a higher $q_{CO_2}$ than the average adsorbent in the literature. As seen in the literature, there exist other activated carbons with higher $CO_2/N_2$ selectivities than those seen in this study.

Binary adsorption isotherms were also predicted for the adsorbents tested at 25°C and 1 atm total pressure using ELM, IAST, and FH-VST for $CO_2$-$N_2$ separation. The predictions from all three models gave similar results. It was seen that at 1 atm total pressure, AC-A had the easiest $CO_2$-$N_2$ separation between the gas and the adsorbed phases from the *x-y* diagram. In terms of the equilibrium adsorption capacities, the activated carbon samples tested are the most appropriate for general use in the separation of $CO_2$ from $N_2$, as they had higher adsorption capacities and also higher $CO_2/N_2$ selectivity values compared to the carbon molecular samples in this study. The activated carbon samples also had similar or higher adsorption capacities and $CO_2/N_2$ selectivity values compared to most of the adsorbents seen from the literature.

## 3.5 Nomenclature

| | |
|---|---|
| $A$ | Surface area of adsorption ($m^2$/kg adsorbent) |
| $B$ | Langmuir parameter ($atm^{-1}$) |
| $b_i$ | Henry's law constant for VST (mol $kg^{-1}$ $atm^{-1}$) |

| | |
|---|---|
| $n$ | Sips parameter (-) |
| $P$ | Pressure (atm) |
| $P^0_i$ | The equilibrium "vapor pressure" for pure i adsorption at the same spreading pressure, π, and the same temperature as the adsorbed mixture (atm) |
| $q$ | Adsorption capacity (mmol $g^{-1}$) |
| $q^0_i$ | Adsorption capacity of pure component i (mmol $g^{-1}$) |
| $q_i^\infty$ | Maximum adsorption capacity for VST model (mmol $g^{-1}$) |
| $q_m$ | Saturation (maximum) adsorption capacity (mmol $g^{-1}$) |
| $q_t$ | Total amount adsorbed (mmol $g^{-1}$) |
| $q_t^\infty$ | Limiting amount adsorbed of mixture (mmol $g^{-1}$) |
| $R$ | Gas constant ($m^3$ atm $K^{-1}$ $mol^{-1}$) |
| $T$ | Temperature (K) |
| $x_i$ | Mole fraction of component i in the adsorbed phase not including the vacancy (-) |
| $x_v$ | Mole fraction of vacancy in the adsorbed phase (-) |
| $x_i^s$ | Mole fraction of component i in adsorbed phase including the vacancy (-) |
| $y_i$ | Mole fraction of component i in the gas phase (-) |

**Greek Symbols**

| | |
|---|---|
| $\alpha_{ij}$ | FH-VST pure component isotherm parameter (-) |
| $\gamma_i^s$ | Activity coefficient of component i (-) |
| $-\Delta H_{ads}$ | Isosteric heat of adsorption (kJ $mol^{-1}$) |
| $\theta$ | Fractional coverage of the adsorbent surface (-) |
| $\pi_i$ | Spreading pressure of component *i* (N/m) |
| $\varphi_i$ | Fugacity coefficient of component i (-) |

**Abbreviations**

| | |
|---|---|
| AC | Activated carbon |
| CMS | Carbon molecular sieve |
| ELM | Extended Langmuir Model |

| | |
|---|---|
| FH | Flory Huggins |
| FH-VST | Flory Huggins-Vacancy Solution Theory |
| GHG | Greenhouse gas |
| IAST | Ideal Adsorbed Solution Theory |
| VST | Vacancy Solution Theory |

## 3.6 References


[1] Intergovernmental Panel on Climate Change, *AR6 Climate Change 2021: The Physical Science Basis,* V. Masson-Delmotte, P. Zhai, A. Pirani, S. L. Connors, C. Péan, S. Berger, N. Caud, Y. Chen, L. Goldfarb, M. I. Gomis, M. Huang, K. Leitzell, E. Lonnoy, J. B. R. Matthews, T. K. Maycock, T. Waterfield, R. Y. O. Yelekçi, B. Zhou, Eds., Cambridge University Press, Cambridge, United Kingdom, **2021**.

[2] Intergovernmental Panel on Climate Change, *AR6 Climate Change 2022: Mitigation of Climate Change*, P. R. Shukla, J. Skea, R. Slade, A. Al Khourdajie, R. van Diemen, D. McCollum, M. Pathak, S. Some, P. Vyas, R. Fradera, M. Belkacemi, A. Hasija, G. Lisboa, S. Luz, J. Malley, Eds., Cambridge University Press, Cambridge, UK, **2022**.

[3] D. Saha, M. J. Kienbaum, *Microporous Mesoporous Mater.* **2019**, *287*, 29.

[4] D. M. D'Alessandro, B. Smit, J. R. Long, *Angew. Chemie - Int. Ed.* **2010**, *49*, 6058.

[5] K. Sumida, D. L. Rogow, J. A. Mason, T. M. McDonald, E. D. Bloch, Z. R. Herm, T. H. Bae, J. R. Long, *Chem. Rev.* **2012**, *112*, 724.

[6] R. T. Yang, *Gas Separation by Adsorption Processes*, Butterworth, Stoneham, MA, **1987**.

[7] A. Wahby, J. M. Ramos-Fernández, M. Martínez-Escandell, A. Sepúveda-Escribano, J. Silvestre-Albero, F. Rodríguez-Reinoso, *ChemSusChem* **2010**, *3*, 974.

[8] Y. Park, D. K. Moon, D. Park, M. Mofarahi, C. H. Lee, *Sep. Purif. Technol.* **2019**, *212*, 952.

[9] L. Predescu, F. H. Tezel, S. Chopra, *Adsorption* **1996**, *3*, 7.

[10] S. Sircar, *J. Chem. Soc. Faraday Trans. 1 Phys. Chem. Condens. Phases* **1985**, *81*, 1527.

[11] H. Pan, J. A. Ritter, P. B. Balbuena, *Ind. Eng. Chem. Res.* **1998**, *37*, 1159.

[12] A. L. Myers, J. M. Prausnitz, *AIChE J.* **1965**, *11*, 121.

[13] T. W. Cochran, R. L. Kabel, R. P. Danner, *AIChE J.* **1985**, *31*, 268.

[14] R. Kapoor, P. Ghosh, M. Kumar, V. K. Vijay, *Environ. Sci. Pollut. Res.* **2019**, *26*, 11631.

[15] Y. Park, D.-K. Moon, Y.-H. Kim, H. Ahn, C.-H. Lee, *Adsorption* **2014**, *20*, 631.

[16] S. M. W. Wilson, F. Al-Enzi, V. A. Gabriel, F. H. Tezel, *Microporous Mesoporous Mater.* **2021**, *322*, 111089.

[17] C. Shen, C. A. Grande, P. Li, J. Yu, A. E. Rodrigues, *Chem. Eng. J.* **2010**, *160*, 398.

[18] J. Park, N. F. Attia, M. Jung, M. E. Lee, K. Lee, J. Chung, H. Oh, *Energy* **2018**, *158*, 9.

[19] J. McEwen, J. D. Hayman, A. Ozgur Yazaydin, *Chem. Phys.* **2013**, *412*, 72.

[20] C. R. Reid, K. M. Thomas, *Langmuir* **1999**, *15*, 3206.

[21] Y. S. Bae, C. H. Lee, *Carbon N. Y.* **2005**, *43*, 95.

# Chapter 4 Binary Adsorption Equilibria of $CO_2$-$N_2$ Mixtures on Activated Carbon

**Dana Li**, Connor Francis, F. Handan Tezel

Department of Chemical and Biological Engineering, University of Ottawa

*161 Louis-Pasteur, Ottawa, Ontario, K1N 6N5 Canada*

## Abstract

The separation of $CO_2$ from $N_2$ by using an activated carbon adsorbent was studied by evaluating the adsorption isotherms of this binary gas mixture. These binary adsorption isotherms were experimentally determined by concentration pulse chromatography in the temperature range of 30 to 70°C for 1 to 5 atm total pressure. The experimental binary isotherms were compared to predictions from single component isotherms using Extended Langmuir Model and the Ideal Adsorbed Solution Theory. The predictive models slightly over predicted the adsorption of $CO_2$ and $N_2$ compared to the experimental data. For the total pressure of 1 atm, the experimental separation of the two gases was better than the predicted separation. However, the experiments at 3 atm and 5 atm demonstrated worse separation than predicted. The difference between the experimental and the model predictions were likely due to competitive adsorption, as indicated by the sharp decrease in effective isotherm slope at low gas phase concentrations of $CO_2$.

**Keywords**

Binary mixture adsorption equilibrium, adsorption, carbon capture, gas separation, carbon dioxide, nitrogen

## 4.1 Introduction

Climate change is a source of major global concern today. Greenhouse gases, of which carbon dioxide is the primary contributor, is responsible for global warming.[1] As such, it is of interest to investigate capture of $CO_2$ emissions. Various separation methods to separate $CO_2$ and $N_2$ have been investigated, especially as it applies to carbon capture and storage. These methods include absorption, ammonia scrubbing, adsorption, cryogenic distillation, and chemical looping.[2] We wanted to look at the adsorption separation of these two gases. This work will be useful in applications of flue gas separation, where $CO_2$ and $N_2$ are the most abundant gases in the mixture.

Activated carbons are low cost adsorbents with high surface area, leading to a high adsorption capacity. Furthermore, they also have high thermal stability and can easily be regenerated.[2,3] In a previous study by Wilson et al., it was found that OLC activated carbon had promising $CO_2/N_2$ ideal selectivity.[4] Thus, this adsorbent was chosen to study in further detail.

The purpose of this study was to study the adsorption separation of $CO_2$ and $N_2$ on OLC activated carbon by determining experimental binary adsorption isotherms, using concentration pulse chromatography.[5–9] $CO_2$-$N_2$ binary adsorption isotherms at 30°C, 50°C, and 70°C at a total system pressure of 1 atm, as well as binary adsorption isotherms at 30°C for 3 atm and 5 atm total pressures were obtained. The experimental binary isotherms were compared to predictions of binary isotherms from the Extended Langmuir Model (ELM) and the Ideal Adsorbed Solution Theory (IAST). A thermodynamic consistency test was also applied to the experimental binary adsorption data.

## 4.2 Materials, Theory and Experimental Methods

### 4.2.1 Materials

OLC 12×30 coconut activated carbon was purchased from Calgon Carbon Corp. (Moon Township, PA, USA). The pellets were crushed to 50×70 US mesh (210-297 μm) size. The gas cylinders used in the binary gas adsorption isotherm experiments were purchased from Messer Canada Inc. (Ottawa, ON, Canada). The activated carbon was exposed to $N_2$ gas (99.999%) and

$CO_2$ gas (99.99%) in these experiments. He gas (99.999%) was used as the purge gas to regenerate the adsorbent at 300°C between changing system operating pressure or temperature.

### 4.2.2 Pure gas adsorption experiments

Pure component gas adsorption isotherm data for activated carbon was collected previously by Wilson et al.[4] using a micro gravimetric analyzer (VTI Corp., acquired from TA Instruments (New Castle, DE, USA) in 2008) equipped with a Cahn microbalance. The experimental data was fitted to various adsorption isotherm models, such as the Langmuir isotherm[10] (Eq. (4.1)) and the Sips isotherm[11] (Eq. (4.2)). These models describe the adsorption capacity $q$ as a function of the pressure $P$. In the Langmuir model, the parameters $q_m$, the monolayer adsorption capacity, and $B$, the equilibrium constant are used. In the Sips isotherm, there is also $n$, which is the number of adsorption sites occupied by an adsorbed molecule.

$$q = \frac{q_m B P}{1 + BP} \tag{4.1}$$

$$\frac{q}{q_m} = \frac{(BP)^{1/n}}{1 + (BP)^{1/n}} \tag{4.2}$$

### 4.2.3 Prediction of binary gas adsorption isotherms from pure component data

#### *4.2.3.1 Extended Langmuir Model*

The ELM equation shown in Eq. (4.3) can be used to predict binary gas adsorption isotherms from the pure component Langmuir model parameters, where $P_i$ indicates the partial pressure of component i in the mixture. It assumes the adsorbent has a uniform surface and there is monolayer adsorption.[12]

$$q_i = \frac{q_{i,m} B_i P_i}{1 + \sum_{j=1}^{n} B_j P_j} \tag{4.3}$$

The amount adsorbed in a binary mixture of component 1 and component 2, $q_1$ and $q_2$ respectively, can be estimated with Eq. (4.4) and (4.5), knowing the Langmuir parameters from the respective pure component model fits.

$$q_1 = \frac{q_1^m B_1 P_1}{1 + B_1 P_1 + B_2 P_2} \tag{4.4}$$

$$q_2 = \frac{q_2^m B_2 P_2}{1 + B_1 P_1 + B_2 P_2} \tag{4.5}$$

#### *4.2.3.2 Ideal Adsorbed Solution Theory*

The IAST is a method of predicting binary adsorption isotherms developed by Myers and Prausnitz. The model assumes an ideal solution and an ideal gas phase, so that an expression analogous to Raoult's law can be applied for the adsorption equilibrium between the gas phase and the adsorbed phase,[13] shown in Eqs. (4.6) and (4.7). The mole fraction of component i in the gas phase is $y_i$ and the mole fraction in the adsorbed phase is $x_i$. $P_i^0$ is the equilibrium pressure for pure component i at the same spreading pressure and the same temperature as the mixture.

$$P y_1 = P_1^0 x_1 \tag{4.6}$$

$$P y_2 = P_2^0 x_2 \tag{4.7}$$

The spreading pressure, $\pi$, of the two components are equal since the mixing is done at constant $\pi$ and can be calculated with the pure component adsorption capacity as shown in Eq. (4.8). $A$ is the surface area of the adsorbent, $q^0_i$ is the adsorption capacity for pure component i, $R$ is the gas constant, and $T$ is the absolute temperature.

$$\int_0^{P_1^0} \frac{q_1^0(P)}{P}\, dP = \frac{\pi_1^0 A}{RT} = \frac{\pi_2^0 A}{RT} = \int_0^{P_2^0} \frac{q_2^0(P)}{P}\, dP \tag{4.8}$$

Because the solution was assumed to be ideal, the specific adsorption area for each adsorbate does not change when they are mixed. Since the specific adsorption area per mole of adsorbate is inversely proportional to amount adsorbed, Eq. (4.9) can be written.[13]

$$\frac{1}{q_t} = \frac{x_1}{q_1^0} + \frac{x_2}{q_2^0} \tag{4.9}$$

### 4.2.4 Binary gas mixture adsorption experiments

Experimental determination of multicomponent gas mixture adsorption properties provides a more realistic indicator of the performance of adsorbents for use in gas separation. Several techniques for the measurement of multicomponent adsorption isotherms have been used in the literature. Of such techniques, concentration pulse chromatography was used in this study. Hyun (1982) has provided a history of development of chromatographic techniques for adsorption measurements.[14] Kipping and Winter (1965) provided an overview of using retention volumes to obtain water adsorption isotherms. Van der Vlist and Van der Meijden (1973) used concentration pulse chromatography to measure binary mixture adsorption isotherms.[5] Shah and Ruthven (1977) and Ruthven and Kumar (1980) also employed concentration pulse chromatography to measure pure gas and binary mixture isotherms.[15,16] Use of the procedure from Van der Vlist and Van der Meijden has been reported previously in the literature,[9,14,17–24] where a good fit for the $K_p$ data is essential for satisfactory binary mixture adsorption isotherm results.[9]

Experimental binary gas adsorption isotherms in this work were determined using concentration pulse chromatography technique. A modified Series 400 gas chromatograph from GOW-MAC Instruments Co. (Bethlehem, PA, USA) with a thermal conductivity detector was used, with a packed adsorbent column inserted. The procedure and experimental setup has been described previously by Kennedy & Tezel.[9]

The adsorbent column used was 3.4 cm long, with an inner diameter of 0.46 cm. Adsorbents were crushed to a mesh size of 50 - 70 US standard mesh (210-297 μm) size and packed into the column. A void fraction of 0.375 was determined by using glass beads of the same mesh size in a graduated cylinder.

The adsorbent was regenerated at 300°C for 15 hours, with He as a purge gas at 1 atm and a 7.4 sccm flowrate. Afterwards, the column was cooled to 30°C, 50°C, or 70°C while He purge

gas continued to pass through the column. When the column was at the desired temperature, He at 6.4 sccm was passed through the column. Three sample injections of $CO_2$ and $N_2$ were inserted into the He carrier, to compare results with the initial slope of the pure component adsorption isotherm data. Afterwards, $N_2$ at 6.4 sccm was passed through the column at 1 atm pressure. The composition of the carrier gas was varied between 0 and 100% $CO_2$ in $N_2$. At each carrier gas composition, three repeated sample injections of $CO_2$ and $N_2$ were done, for a total of six sample injections per composition. The error bars from the experiments show the range of data collected from the six injections.

The apparent equilibrium constant, which is the combined slope of the two binary isotherms in the mixture, was determined by using the concentration pulse chromatography technique.[5] The mean retention time (first moment of the response peak) for a small volume of sample gas to pass through the adsorbent column was used to determine the dimensionless apparent equilibrium constant ($K$). This mean retention time ($\mu$) was determined by analyzing the experimental response peak knowing concentration ($c$), the dead volume time ($\mu_d$), and time ($t$), and by carrying out the integrations shown on the left hand side of Eq. (4.10). It is related to $K$ using the column length ($L$), interstitial velocity in the column ($v$), and the bed porosity ($\varepsilon$) as shown in Eq. (4.10).[16] After the determination of the dimensionless apparent equilibrium constant, $K$, using Eq. (4.10), it was converted to its dimensional form, $K_p$, using Eq. (4.11) where $\rho_s$ is the density of the solid adsorbent.

$$\mu = \frac{\int_0^\infty c(t-\mu_d)dt}{\int_0^\infty c\,dt} = \frac{L}{v}\left[1 + \frac{(1-\varepsilon)K}{\varepsilon}\right] \tag{4.10}$$

$$K_p = \frac{K}{RT\rho_s} \tag{4.11}$$

The contribution of the two components in the gas mixture to the overall dimensional apparent equilibrium constant as shown by Eq. (4.12).[5] The slope of the binary adsorption isotherm for component i in the binary mixture is represented by $dq_i/dP_i$.

$$K_p = (1 - y_1)\frac{dq_1}{dP_1} + y_1\frac{dq_2}{dP_2} \tag{4.12}$$

Various models have been proposed for relating the $K_p$ value to the mole fraction of component 1 in the gas phase, $y_1$. The most important criteria for the success of determining binary adsorption isotherms using concentration pulse chromatography technique is to find the best model to represent the experimental $K_p$ vs. $y_1$ data. The Harlick and Tezel Concentration Pulse Method (HT-CPM)[7,8,18,19,21,25] was used in this work because it provided the most accurate model representation of the experimental data compared to other models such as the modified Van der Vlist and Van der Meijden model,[5,20,22–24,26] the modified Triebe and Tezel-concentration pulse model,[6,7] and the Kennedy and Tezel-concentration pulse model.[9] As such, only the HT-CPM will be discussed in further detail. HT-CPM is a five-parameter function ($A_1$-$A_4$, $\lambda$),[8] as shown in Eq. (4.13).

$$K_p = A_1 + A_2 y_1 + A_3 y_1^2 + A_4 \ln|y_1 + \lambda| \tag{4.13}$$

The derivative of Eq. (4.13) gives the equation for the slope of the binary adsorption isotherms as a function of $y_1$. This is shown in Eqs. (4.14) and (4.15) for components 1 and 2, respectively, where $B_1$-$B_3$ and $C_1$-$C_3$ are also parameters.

$$\frac{dq_1}{dP_1} = B_1 + 2B_2 y_1 + \frac{B_3}{|y_1 + \lambda|} \tag{4.14}$$

$$\frac{dq_2}{dP_2} = C_1 + 2C_2 y_1 + \frac{C_3}{|y_1 + \lambda|} \tag{4.15}$$

The binary isotherm slope equations from Eqs. (4.14) and (4.15) can be substituted into Eq. (4.12) to obtain Eq. (4.16).

$$K_p = (1 - y_1)\left[B_1 + 2B_2 y_1 + \frac{B_3}{|y_1 + \lambda|}\right] + y_1\left[C_1 + 2C_2 y_1 + \frac{C_3}{|y_1 + \lambda|}\right] \tag{4.16}$$

This can be used to fit the experimental $K_p$ vs. $y_1$ data to find the six unknown parameters, $B_1$ to $B_3$ and $C_1$ to $C_3$, by minimizing the overall sum of square residuals (SSR) using Eq. (4.17).

$$SSR = \sum_{j=1}^{n} (K_{p,j\ experimental} - K_{p,j\ model})^2 \tag{4.17}$$

By integrating Eq. (4.14) and (4.15), after the determination of $B$ and $C$ parameters, the adsorption capacity of each component in the binary mixture, $q_1$ and $q_2$, can be calculated using Eqs. (4.18) and (4.19).

$$q_1 = P_T \left[ B_1 y_1 + B_2 y_1^2 + B_3 \ln \left| \frac{y_1 + \lambda}{\lambda} \right| \right] \tag{4.18}$$

$$q_2 = P_T \left[ C_1 (1 - y_1) + C_2 (1 - y_1^2) - C_3 \ln \left| \frac{y_1 + \lambda}{1 + \lambda} \right| \right] \tag{4.19}$$

In order for the fitted model to have physical meaning, two constraints were imposed in the Solver function of Excel so that the $K_p$ values of the fitted expression pass through the experimental $K_p$ values at the two boundaries for the composition when $y_1$=0 and $y_1$=1, as shown in Eqs. (4.20) and (4.21).[7]

$$K_{p,exp}|_{y_1=0} = K_{p,fit}|_{y_1=0} \tag{4.20}$$

$$K_{p,exp}|_{y_1=1} = K_{p,fit}|_{y_1=1} \tag{4.21}$$

Furthermore, there should be no maximum observed in the isotherm, so the slope of the isotherm should always be positive.[27] There were no constraints imposed on the adsorption capacity at $y_1$=0 and $y_1$=1 while fitting the model.

Other than the adsorption capacity, another performance criterion for adsorbents is the separation factor (Eq. (4.22)). This gives an indication of the adsorbent's ability to separate gases in a mixture.

$$Separation\ factor = \frac{x_1/x_2}{y_1/y_2} \tag{4.22}$$

### 4.2.5 Thermodynamic Consistency Test

The Gibbsian Surface Excess model has been used to investigate the thermodynamics of pure and multicomponent gas adsorption isotherms and can be used to check the thermodynamic consistency of the binary gas isotherms. Integral and differential tests have been developed to check the consistency using the pure and binary isotherm data.[28] The integral thermodynamic consistency test (Eq. (4.23)) was used in this work.

$$-\int_0^P \frac{q_2^o}{P}\,dP - \left(-\int_0^P \frac{q_1^o}{P}\,dP\right) = \int_0^1 \frac{q_1(1-y_1) - q_2 y_1}{y_1(1-y_1)}\,dy_1 \tag{4.23}$$

The left hand side (LHS) of the equation is calculated from the pure component isotherm data, while the right hand side (RHS) is calculated with the binary isotherm data. The percentage difference between the LHS and RHS of the equation gives an indication of the thermodynamic consistency of the binary adsorption data.

## 4.3 Results and Discussion

### 4.3.1 $K_p$ for $CO_2$-$N_2$ mixture

The experimental average $K_p$ values as functions of the gas phase $CO_2$ concentration were plotted in Figure 4.1 for different operating conditions, together with their HT-CPM model comparisons. Figure 4.1 (a) shows $K_p$ as a function of mole fraction of $CO_2$ in the carrier gas at total pressures of 1, 3, and 5 atm and 30°C while Figure 4.1 (b) shows $K_p$ as a function of mole

fraction of $CO_2$ in the carrier gas at 30, 50, and 70°C, at a total pressure of 1 atm. The HT-CPM model was found to fit the experimental data the best and was used to model all experimental data presented in this work. When pure sample gas is injected into the column, there is a small increase in the concentration of the gas injected, allowing the measurement of the experimental $K_p$. Because separate injections with $N_2$ and injections with $CO_2$ were done at each concentration, an average of these values was used for the analysis. This analysis would minimize the effect of the small change in concentration as a result of sample injection.[16] The error bars represent the range of experimental $K_p$ values obtained. The parameters fit to the HT-CPM model are shown in Table 4.1.

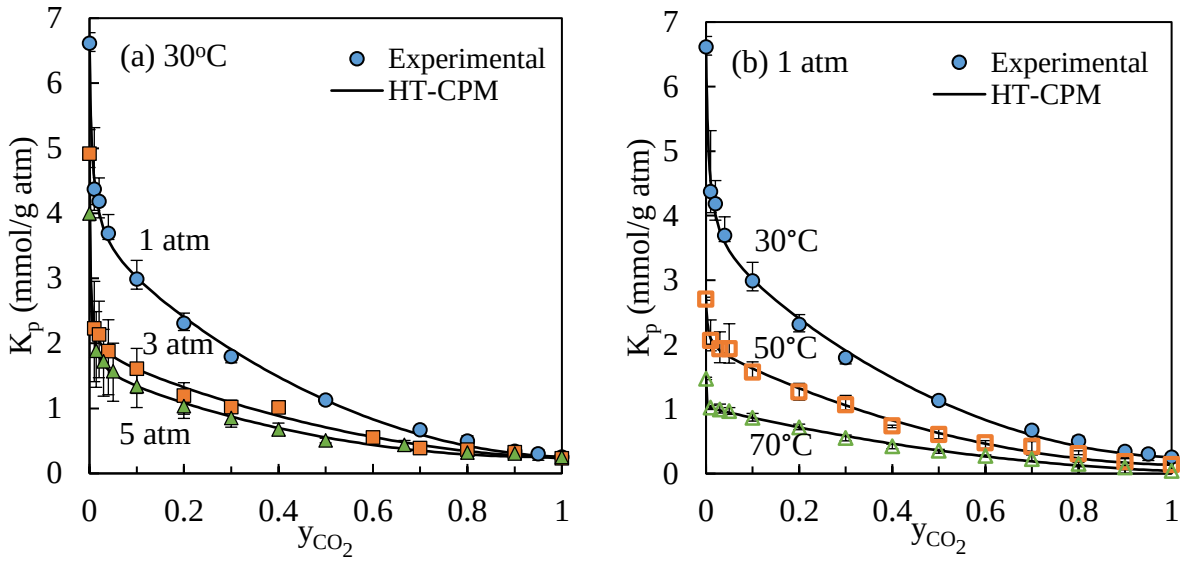


Figure 4.1 Experimental $K_p$ values for $CO_2$ and $N_2$ gas mixture on OLC, as a function of mole fraction of $CO_2$ in the gas, $y_{CO_2}$, and their comparison to HT-CPM model (a) at 30°C at 1-5 atm total pressure and (b) at 1 atm total pressure at 30-70°C.

For all experimental conditions, the value of $K_p$ sharply decreased at concentrations of $CO_2$ lower than $y_{CO_2}$ = 0.2. From $y_{CO_2}$ = 0.2 to $y_{CO_2}$ = 0.8, $K_p$ decreased almost linearly. Finally, from $y_{CO_2}$ = 0.8 to $y_{CO_2}$ = 1.0, $K_p$ decreased very slightly and remained almost constant in the case of 3 atm and 5 atm. The sharp decrease in the $K_p$ at $y_{CO_2}$ lower than 0.2 is suggestive of competition for adsorption sites.[25]

Table 4.1 HT-CPM Parameters for experimental $K_p$ values.

| | 30°C, 1 atm | 30°C, 3 atm | 30°C, 5 atm | 50°C, 1 atm | 70°C, 1 atm |
|---|---|---|---|---|---|
| $B_1$ (mmol $g^{-1}$ $atm^{-1}$) | 3.444 | 1.832 | 1.530 | 1.931 | 1.025 |
| $B_2$ (mmol $g^{-1}$ $atm^{-1}$) | -1.349 | -0.542 | -0.589 | -0.745 | -0.329 |
| $B_3$ (mmol $g^{-1}$ $atm^{-1}$) | 1.82E-02 | 5.90E-03 | 7.47E-03 | 2.74E-03 | 2.04E-04 |
| $C_1$ (mmol $g^{-1}$ $atm^{-1}$) | -4.07E-03 | -2.82E-03 | 4.48E-02 | -1.88E-03 | -4.26E-04 |
| $C_2$ (mmol $g^{-1}$ $atm^{-1}$) | 1.29E-01 | 1.18E-01 | 1.06E-01 | 6.93E-02 | 2.03E-02 |
| $C_3$ (mmol $g^{-1}$ $atm^{-1}$) | 2.34E-05 | 5.39E-06 | -1.35E-04 | 6.65E-06 | 1.94E-07 |
| λ (-) | 5.75E-03 | 1.91E-03 | 3.02E-03 | 3.54E-03 | -4.56E-04 |
| SSR (mmol $g^{-1}$ $atm^{-1}$) | 0.100 | 0.058 | 0.018 | 0.045 | 0.006 |

As the pressure increased from 1 atm to 5 atm, as shown in Figure 4.1 (a), the $K_p$ values decreased. At higher pressures, the slope of the adsorption isotherm becomes less steep, so this trend was expected, as this trend can be observed for the pure component isotherms. Even though the $K_p$ values were higher at 1 atm compared to 5 atm, the amount adsorbed increased from 1 atm to 5 atm.

As the temperature increased from 30°C to 70°C, as shown in Figure 4.1 (b), the $K_p$ values decreased. This was expected as well, since the isotherm slope, and the amount adsorbed decrease as the temperature increases. This trend is similar to that is shown in the pure component isotherms.[4]

### 4.3.2 $CO_2$-$N_2$ binary isotherm and comparison to predictions

Using the fitted HT-CPM parameters in Table 4.1 and Eqs. (4.18) and (4.19), the experimental binary adsorption isotherms were determined and are shown in Figure 4.2. The adsorption capacity values of $CO_2$ and $N_2$ at 1 atm pressure from pure component adsorption isotherm data (shown as blue dots for $CO_2$ and orange dots for $N_2$), as well as the predictions of the binary adsorption isotherms from ELM and IAST models were also plotted on this figure for comparison.

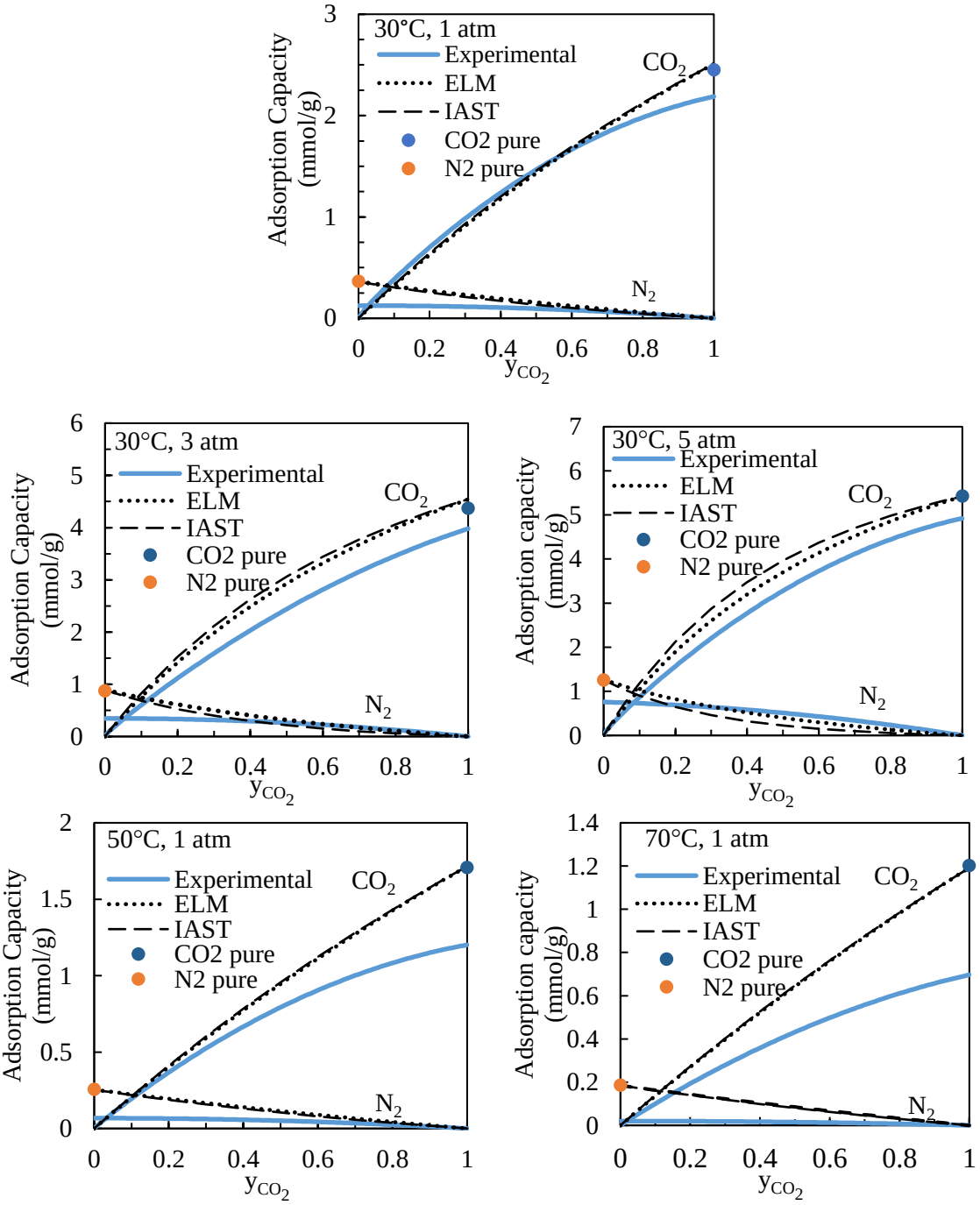


Figure 4.2 Binary adsorption isotherms of $CO_2$-$N_2$ gas mixture with OLC adsorbent at 30-50°C and 1-5 atm total pressure and their comparisons to pure component amounts adsorbed at the same pressure and temperature.

In general, both $CO_2$ and $N_2$ adsorption capacities were over predicted by IAST and ELM at the experimental conditions tested. This meant that the adsorption capacities in the binary mixture were lower than the pure component adsorption capacities and indicated the non-ideality

of the binary mixture adsorption. At 3 atm and 5 atm, it was observed that the experimental amount of $N_2$ adsorbed was slightly higher than that predicted at higher concentrations of $CO_2$. As the temperature increased from 30°C to 70°C, the difference between the predictions and the experimental data increased as well. Therefore, it was observed that the predictions from single component data were not sufficient to predict the behaviour of the binary adsorption system.

As $y_{CO_2}$ increased, the amount of $CO_2$ adsorbed increased as expected. Furthermore, the amount of $N_2$ adsorbed decreased at higher $y_{CO_2}$. As $y_{CO_2}$ increased, $q_{CO_2}$ increased greatly. However, as $y_{CO_2}$ increased, $q_{N_2}$ did not decrease at a large rate because the $N_2$ adsorption was low. Like the trend in the $K_p$ values, the amount of both $N_2$ and $CO_2$ adsorbed also decreased as the temperature increased, which was expected since physical adsorption is an exothermic process. With increasing pressure, the amounts adsorbed for both $CO_2$ and $N_2$ increased, as expected.

It should be noted that the experimental binary $N_2$ isotherm in the $CO_2$-$N_2$ binary mixture at $y_{CO_2} = 0$ did not correspond to the amount for pure $N_2$ is adsorbed from pure component isotherms at 1 atm (orange dot). The same can be said for the $CO_2$ isotherm in the $CO_2$-$N_2$ binary mixture at $y_{CO_2} = 1$ compared to the amount of pure $CO_2$ adsorbed at 1 atm (blue dot). This can be explained by the fact that for the binary mixture experiment at $y_{CO_2} = 0$, a small sample of $CO_2$ was injected into a carrier stream of pure $N_2$ to obtain a response peak, meaning a quantity at infinite dilution was being measured, and not the pure component. Similarly, at $y_{CO_2} = 1$, a small sample of $N_2$ is injected into a carrier stream of pure $CO_2$, indicating the infinite dilution of the system, as opposed to the pure component. Thus, the fact that pure amount $N_2$ and $CO_2$ adsorbed (orange or blue dots, respectively) do not correspond to the amount of $N_2$ or $CO_2$ adsorbed in the binary mixture isotherms (blue curves) at the two boundaries for the composition, indicate the non-ideality of the mixture. On the other hand, the pure component adsorption capacities for both gases coincided with the end points of the ELM and IAST predictions, as they should, since both ELM and IAST assume ideal mixtures.

The binary gas mixture experiments showed that there was deviation from the predictions from IAST and ELM. Thus, some caution should be taken if using these prediction models for $CO_2$-$N_2$ adsorption on OLC activated carbon. In general, predictions from single component isotherm data are often inadequate for highly selective binary systems.[7,9,24]

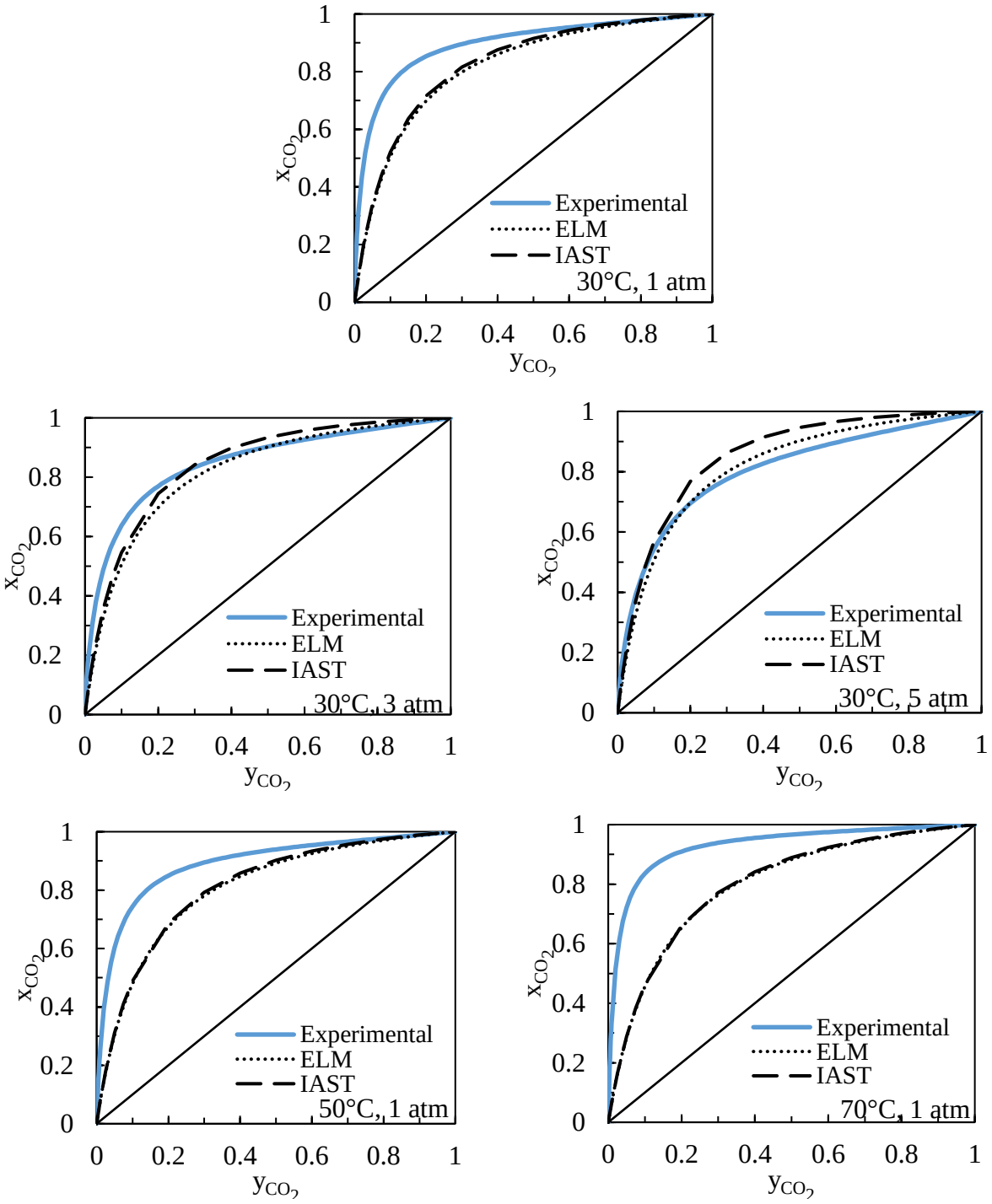


Figure 4.3 Phase diagram of mole fraction of $CO_2$ in adsorbed phase vs. mole fraction of $CO_2$ in the feed gas for $CO_2$-$N_2$ binary experiments on OLC.

In Figure 4.3, the phase diagrams for the $CO_2$-$N_2$ binary system were plotted. There was better separation at lower pressure, which can be seen as the curve is further away from the 45°

line at 1 atm. Previously, it has been observed that selectivity decreases with increasing pressure due to capacity limits in the adsorbent at higher loading in activated carbon Xtrusorb A754, silica gel SG-B127, and 13X zeolite,[23] which corresponds to the same trends seen with OLC activated carbon as the total pressure increased. At higher temperature, however, the separation was better. At most of the experimental conditions tested, the experimental separation was greater than the predicted separation. The exceptions were at 3 atm, when $y_{CO_2} > 0.4$, and at 5 atm, where the curve for the experimental data was closer to the 45° line than the predictions.

The separation factor values for $CO_2/N_2$ adsorption separation with adsorbent OLC at 30-70°C for total pressure of 1 atm. and at 1-5 atm total pressure for 30°C were calculated from Eq. (4.22) and are shown in Figure 4.4, as a function of gas phase composition. As the total pressure increased, the separation factors decreased, which match the trends seen in the *x-y* diagrams in Figure 4.3. From 30°C to 50°C, the separation factors were very similar, with 30°C being slightly higher. However, the highest separation factors were observed at 1 atm total pressure and 70°C. Even though the separation factor improved from 30°C to 70°C, adsorption capacities halved.

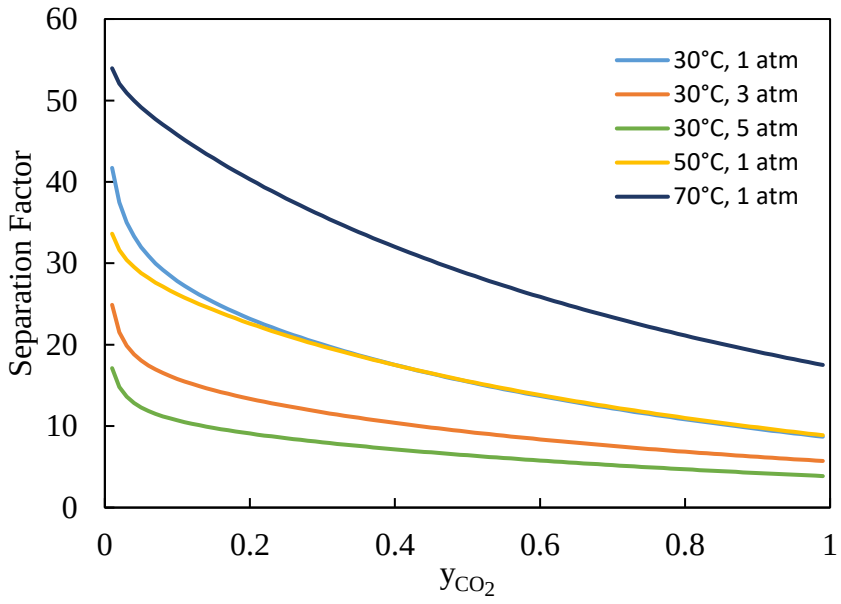


Figure 4.4 Separation factor values for $CO_2/N_2$ adsorption separation with adsorbent OLC at 30, 50, 70°C for 1 atm, total pressure and at 1, 3, 5 atm total pressure for 30°C.

### 4.3.3 Thermodynamic Consistency

The results of the thermodynamic consistency test in Eq. (4.23) are shown in Table 4.2. As can be seen, the percentage difference between the LHS, using the pure component data, and RHS, using the experimental binary mixture data, of the integral test was moderate, ranging from 11% to 38%. As temperature increased, so did the percent difference. As the pressure increased, the percent difference also increased. These trends coincide with the experimental deviation from predictive models, where there was a larger difference between the two at higher temperatures and higher pressures.

Table 4.2 Thermodynamic consistency test results

| | 30°C, 1 atm | 30°C, 3 atm | 30°C, 5 atm | 50°C, 1 atm | 70°C, 1 atm |
|---|---|---|---|---|---|
| LHS | 3.17 | 6.10 | 8.01 | 2.05 | 1.33 |
| RHS | 2.81 | 4.44 | 5.74 | 1.49 | 0.83 |
| % difference | 11.38 | 27.12 | 28.28 | 27.32 | 37.88 |

### 4.3.4 Comparison to Other Adsorbents

The $CO_2$-$N_2$ binary adsorption of OLC was compared with the performance of other adsorbents in the literature at 40°C and 1 atm total pressure: H-ZSM-5-30,[8] H-ZSM-5-280,[8] Silicalite,[9] and Ceca 13X.[21] It was also compared to activated carbon Filtrasorb 400 at 40°C and approximately 0.8 atm total pressure.[29] These comparisons are shown in Figure 4.5. While data for OLC was collected at 30°C and 50°C but not 40°C, it was still possible to see that H-ZSM-5-30 and 13X at 40°C had a better $CO_2$ adsorption capacity. The adsorption capacity of OLC was comparable to that of H-ZSM-5-280 and silicalite. Of the adsorbents shown here, Filtrasorb 400 had the highest $CO_2$ adsorption capacity, but also a high $N_2$ adsorption capacity.

In Figure 4.6, the separation factor calculated using Eq. (4.22) of OLC is compared to the other adsorbents from Figure 4.5 from the literature. At very low $y_{CO_2}$, up to about 0.01, Ceca 13X had the highest separation factor. Otherwise, OLC at 30°C had the highest separation factor for $CO_2$-$N_2$ binary gas adsorption. The separation factors of OLC at 30°C and 50°C were very similar,

so even though the other adsorbents shown in Figure 4.6 were tested at 40°C, it can be seen that OLC had higher separation factors than them.

For direct air capture applications, where the concentration of $CO_2$ is extremely low, 13X would be the most appropriate adsorbent for separation between $CO_2$ and $N_2$, of the adsorbents discussed here due to high $CO_2$ adsorption capacity and $CO_2/N_2$ separation factor at those conditions. However, for combustion flue gas applications and use in biogas $CO_2$ capture, where concentrations of $CO_2$ are higher, H-ZSM-5-30 would provide the best $CO_2$ adsorption capacity, but OLC would provide the best separation factor between $CO_2$ and $N_2$.

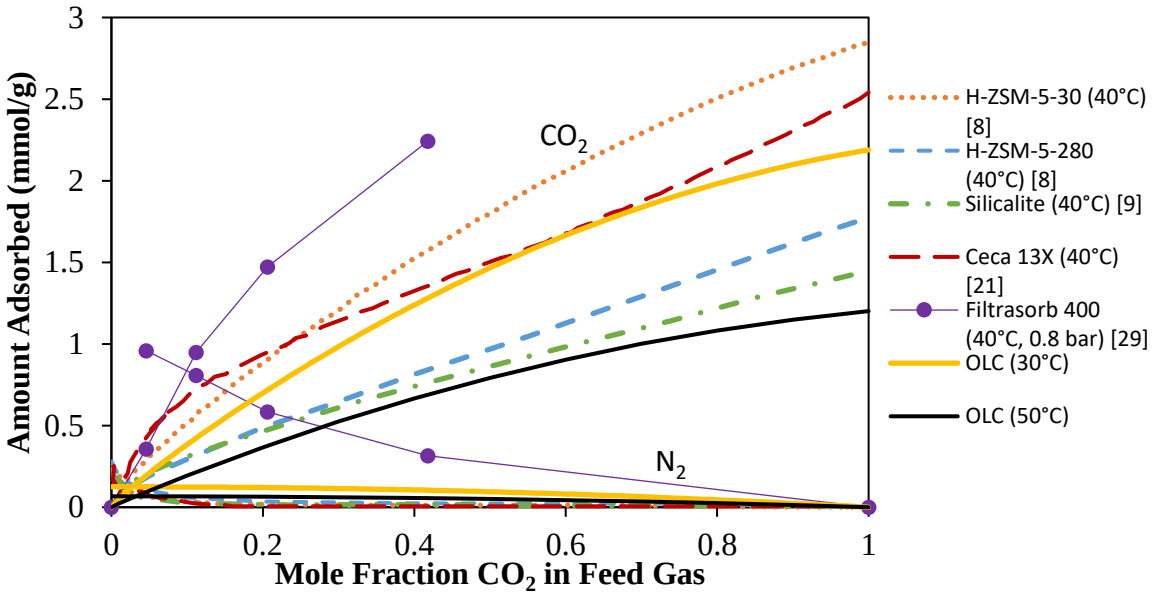


Figure 4.5 Comparison of $CO_2$-$N_2$ binary gas adsorption between OLC at 30°C and 50°C at 1 atm total pressure (this work), H-ZSM-5-30,[8] H-ZSM-5-280,[8] silicalite,[9] and Ceca 13X[21] at 40°C and 1 atm total pressure, and Filtrasorb 400[29] at 40°C and 0.8 atm total pressure

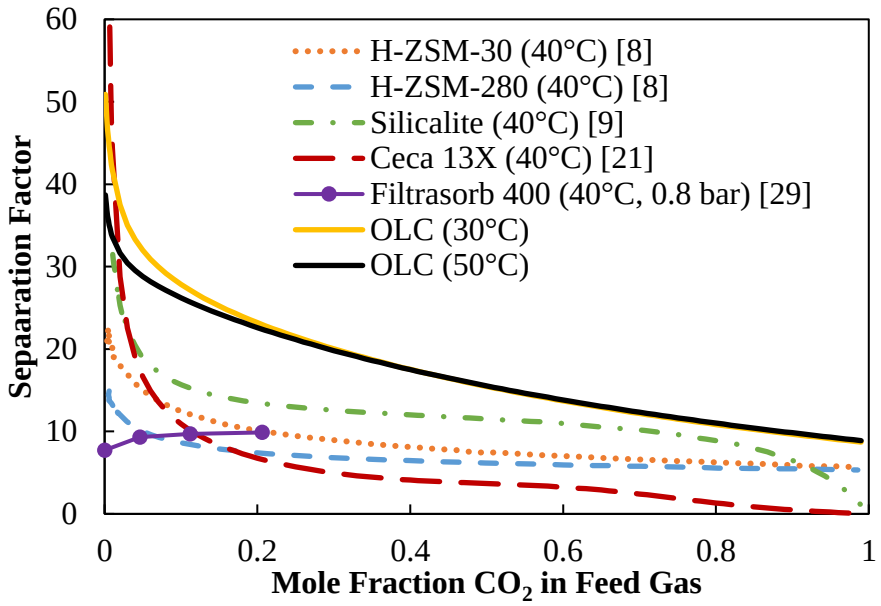


Figure 4.6 Comparison of separation factors for H-ZSM-5-30,[8] H-ZSM-5-280,[8] silicalite,[9] Ceca 13X at 40°C and 1 atm total pressure,[21] Filtrasorb 400[29] at 40°C and 0.8 atm total pressure, and OLC at 30°C and 50°C at 1 atm total pressure from this study for $CO_2$-$N_2$ binary gas adsorption.

## 4.4 Conclusions

Experimental $CO_2$-$N_2$ binary adsorption isotherms at 30 to 70°C and at 1 to 5 atm total pressure on a commercial activated carbon OLC were determined using concentration pulse chromatography technique using the model from HT-CPM. The experimental binary isotherms were compared to the predictions from ELM and IAST models. It was found that these models were not able to accurately predict the experimental data, with sharp decline of $K_p$ at low $CO_2$ gas phase concentrations suggesting competitive adsorption.

The $CO_2$-$N_2$ separation was the worse at lower temperatures and at higher pressures, as seen by the *x-y* diagrams and the separation factors. The amount of $CO_2$ and $N_2$ adsorbed also decreased at higher temperatures. However, there was an increase in amount of $CO_2$ and $N_2$ adsorbed at higher pressures. This demonstrated the importance of both temperature and pressure in the performance of this activated carbon.

Compared to other adsorbents in literature such as 13X and silicalite, the adsorption capacity of OLC was comparable. However, OLC was observed to have higher $CO_2$-$N_2$ separation

factor than those presented. OLC appears to be a promising adsorbent for use in $CO_2$ and $N_2$ separations.

## 4.5 Nomenclature

| | |
|---|---|
| $A$ | Specific area of adsorbent ($m^2$/kg adsorbent) |
| $A_1$, $A_2$, $A_3$, $A_4$ | Parameters for HT-CPM (mmol $g^{-1}$ $atm^{-1}$) |
| $B$ | Langmuir parameter ($atm^{-1}$) |
| $B_1$, $B_2$, $B_3$ | Parameters for HT-CPM (mmol $g^{-1}$ $atm^{-1}$) |
| $c$ | Concentration (mol $m^{-3}$) |
| $C_1$, $C_2$, $C_3$ | Parameters for HT-CPM (mmol $g^{-1}$ $atm^{-1}$) |
| $K$ | Dimensionless apparent equilibrium constant (-) |
| $K_p$ | Dimensional apparent equilibrium constant (mmol $g^{-1}$ $atm^{-1}$) |
| $L$ | Column length (m) |
| $n$ | Sips parameter (-) |
| $P$ | Pressure (atm) |
| $P^0_i$ | Equilibrium pressure at the same adsorption capacity as the spreading pressure (atm) |
| $R$ | Gas constant ($m^3$ atm $K^{-1}$ $mol^{-1}$) |
| $q$ | Adsorption capacity (mmol $g^{-1}$) |
| $q^0_i$ | Adsorption capacity of pure component i (mmol $g^{-1}$) |
| $t$ | Time (s) |
| $T$ | Temperature (K) |
| $v$ | Interstitial velocity (m $s^{-1}$) |
| $x_i$ | Mole fraction of component i in the adsorbed phase (-) |
| $y_i$ | Mole fraction of component i in the gas phase (-) |

**Greek Letters**

| | |
|---|---|
| $\varepsilon$ | Adsorbent bed porosity (-) |
| $\lambda$ | Parameter for HT-CPM (-) |

$\mu$ Mean retention time (s)

$\mu_D$ Dead volume time (s)

$\pi$ Spreading pressure (N/m)

$\rho_s$ Solid density (kg $m^{-3}$)

**Abbreviations**

| | |
|---|---|
| ELM | Extended Langmuir Model |
| HT-CPM | Harlick and Tezel Concentration Pulse Method |
| IAST | Ideal Adsorbed Solution Theory |
| LHS | Left hand side |
| RHS | Right hand side |
| SSR | Sum of square residuals |

## 4.6 References


[1] U. Kamran, S. J. Park, *J. Clean. Prod.* **2021**, *290*, 125776.

[2] J. Godin, W. Liu, S. Ren, C. C. Xu, *J. Environ. Chem. Eng.* **2021**, *9*, 105644.

[3] D. Peredo-Mancilla, C. Matei Ghimbeu, B. N. Ho, M. Jeguirim, C. Hort, D. Bessieres, *J. Environ. Chem. Eng.* **2019**, *7*, 103368.

[4] S. M. W. Wilson, F. Al-Enzi, V. A. Gabriel, F. H. Tezel, *Microporous Mesoporous Mater.* **2021**, *322*, 111089.

[5] E. van der Vlist, J. van der Meijden, *J. Chromatogr.* **1973**, *79*, 1.

[6] R. W. Triebe, F. H. Tezel, *Can. J. Chem. Eng.* **1995**, *73*, 717.

[7] P. J. E. Harlick, F. H. Tezel, *Adsorption* **2000**, *6*, 293.

[8] P. J. E. Harlick, F. H. Tezel, *Can. J. Chem. Eng.* **2001**, *79*, 236.

[9] D. Kennedy, F. H. Tezel, *Adsorption* **2014**, *20*, 189.

[10] I. Langmuir, *J. Am. Chem. Soc.* **1918**, *40*, 1361.

[11] R. Sips, *J. Chem. Phys.* **1948**, *16*, 490.

[12] E. C. Markham, A. F. Benton, *J. Am. Chem. Soc.* **1931**, *53*, 497.

[13] A. L. Myers, J. M. Prausnitz, *AIChE J.* **1965**, *11*, 121.

[14] S. H. Hyun, Gas-Mixture Adsorption Isotherms and Diffusivities in Molecular Sieves by Perturbation Chromatography, Pennsylvania State University, **1982**.

[15] D. B. Shah, D. M. Ruthven, *AIChE J.* **1977**, *23*, 804.

[16] D. M. Ruthven, R. Kumar, *Ind. Eng. Chem. Fundam.* **1980**, *19*, 27.

[17] F. H. Tezel, H. O. Tezel, D. M. Ruthven, *J. Colloid Interface Sci.* **1992**, *149*, 197.

[18] P. Li, F. H. Tezel, *Sep. Sci. Technol.* **2007**, *42*, 3131.

[19] P. Li, F. H. Tezel, *J. Chem. Eng. Data* **2008**, *53*, 2479.

[20] P. Li, F. H. Tezel, *J. Chem. Eng. Data* **2009**, *54*, 8.

[21] V. P. Mulgundmath, F. H. Tezel, T. Saatcioglu, T. C. Golden, *Can. J. Chem. Eng.* **2012**, *90*, 730.

[22] V. P. Mulgundmath, F. H. Tezel, F. Hou, T. C. Golden, *J. Porous Mater.* **2012**, *19*, 455.

[23] D. A. Kennedy, M. Mujcin, E. Trudeau, F. H. Tezel, *J. Chem. Eng. Data* **2016**, *61*, 3163.

[24] D. A. Kennedy, M. Mujčin, T. Alenko, F. H. Tezel, *Adsorption* **2019**, *25*, 135.

[25] P. J. E. Harlick, F. H. Tezel, *Sep. Purif. Technol.* **2003**, *33*, 199.

[26] M. J. Heslop, B. A. Buffham, G. Mason, *Ind. Eng. Chem. Res.* **1996**, *35*, 1456.

[27] G. Calleja, J. Pau, J. A. Calles, *J. Chem. Eng. Data* **1998**, *43*, 994.

[28] M. B. Rao, S. Sircar, *Langmuir* **1999**, *15*, 7258.

[29] M. Sudibandriyo, Z. Pan, J. E. Fitzgerald, R. L. Robinson Jr., K. A. M. Gasem, *Langmuir* **2003**, *19*, 5323.

# Chapter 5 - Conclusions and Recommendations for Future Work

## 5.1 Overall Conclusions

First, the reliability of concentration pulse chromatography (CPC) technique was evaluated for determining pure component adsorption isotherms by comparing $CH_4$ isotherm results for activated carbon to data collected using a micro-gravimetric system. It was found that using a column that was too short led to an overestimation of the adsorption capacity, as the isotherms from the 3.4 cm and 8.7 cm long columns gave erroneous results. However, isotherm obtained using CPC with the 15 cm column coincided with the isotherm obtained using the gravimetric technique. Furthermore, the effect of carrier gas total flowrate was investigated, and in the study it appeared that flowrate did not have a significant effect on the isotherm measurement using the 15 cm column, as expected. Using the correct experimental conditions, such as a sufficiently long column, CPC can be used to measure pure component isotherms.

Second, the $CO_2$ and $N_2$ adsorption capacities of three commercially available activated carbons and four carbon molecular sieves were measured gravimetrically. Out of these adsorbents, the activated carbons exhibited higher adsorption capacities than the carbon molecular sieves. At 9.7 atm, AC-B had an adsorption capacity of 7.5 mmol/g, which was the highest for the adsorbents tested. Predictions of the binary adsorption isotherms at 1 atm showed that AC-A had the best separation between $CO_2$ and $N_2$. All the adsorbents tested demonstrated an equilibrium selectivity for $CO_2$ over $N_2$ though.

Third, experimental $CO_2$-$N_2$ binary gas adsorption isotherms for OLC activated carbon were measured using CPC between 30-70°C and 1-5 atm total pressure. A slight difference between the experimental binary adsorption isotherms and their predictions were found. While adsorbents such as 13X and ZSM-5 may have higher $CO_2$ adsorption capacities in a $CO_2$-$N_2$ mixture, OLC demonstrated high $CO_2/N_2$ selectivity compared to other adsorbents in the literature.

## 5.2 Recommendations for Future Work

Several recommendations came out of this work, to further the understanding of adsorption behaviour:

- Determine a set of criteria necessary for reliable concentration pulse chromatography experiments that can be consulted before starting experiments.
- Study the adsorbents' physical properties, such as pore size distribution and BET surface area, to describe the trends observed in the adsorption capacities.
- Investigate the $CH_4$ adsorption properties of the activated carbons in Chapter 3, as these could not be completed due to fumehood requirements.
- Calculate the activity coefficients for the binary adsorption isotherm results, as the experimental isotherms showed discrepancy from the theoretical predictions.